Results

Dorfin reduces the levels of total, cytosolic and mitochondrial mutant SOD1

Confocal laser scanning microscopic images revealed that expression of both non-organelle-oriented Cyto-SOD1 plasmid and pcDNA3.1/HisMax-Dorfin was diffusely present in the cells. SOD1-EGFP fusion proteins were co-localized with Xpress-Dorfin fusion proteins (Figs 1a–i), consistent with our previous study (Niwa *et al.* 2002; Takeuchi *et al.* 2002a). In contrast, the expression of mitochondria-oriented Mito-SOD1 plasmid was observed in the mitochondria, as in our previous report (Takeuchi *et al.* 2002a), and was not co-localized with Xpress-Dorfin fusion proteins (Figs 1j–l). Western blots also revealed that Xpress-Dorfin fusion proteins were absent from the mitochondrial fraction (Fig. 1m). At 48 h after transfection, co-expression of Dorfin had reduced the total cell lysate level of SOD1-EGFP fusion proteins expressed by Cyto-G93A or Cyto-G85R by approximately 40%, whereas it did not affect those expressed by Cyto-WT (Fig. 2). In contrast, the amount of SOD1-EGFP fusion proteins expressed by Mito-SOD1 did not show any reduction even with co-expression of Dorfin (Fig. 2). In the cytosolic fraction, co-expression of Dorfin also reduced the level of SOD1-EGFP fusion proteins expressed by Cyto-G93A or Cyto-G85R by approximately 40%, whereas it did not affect those expressed by Cyto-WT (Fig. 3). As we described previously (Takeuchi *et al.* 2002a), cells with Mito-SOD1 showed very small amounts of SOD1-EGFP fusion proteins in the cytosolic fraction (Fig. 3). In the mitochondrial fraction, co-expression of Dorfin also reduced the level of SOD1-EGFP fusion proteins expressed by Cyto-G93A or Cyto-G85R by approximately 50%, whereas it did not affect those expressed by Cyto-WT (Fig. 4). This reduction in mitochondrial SOD1-EGFP was observed from 24 h after transfection, earlier than that of total or cytosolic SOD1-EGFP. In contrast, in the cells with Mito-SOD1, Dorfin did not reduce the amount of mitochondrial SOD1-EGFP fusion proteins (Fig. 4). The above results suggest that the mitochondrial accumulation of mutant SOD1 without organelle-oriented signals might be a result of mutant SOD1 in the cytosol, and we suggest that Dorfin, a cytosolic E3, reduced the accumulation of mutant SOD1 in the mitochondria by enhancing the degradation of mutant SOD1 in the cytosol, not in the mitochondria.

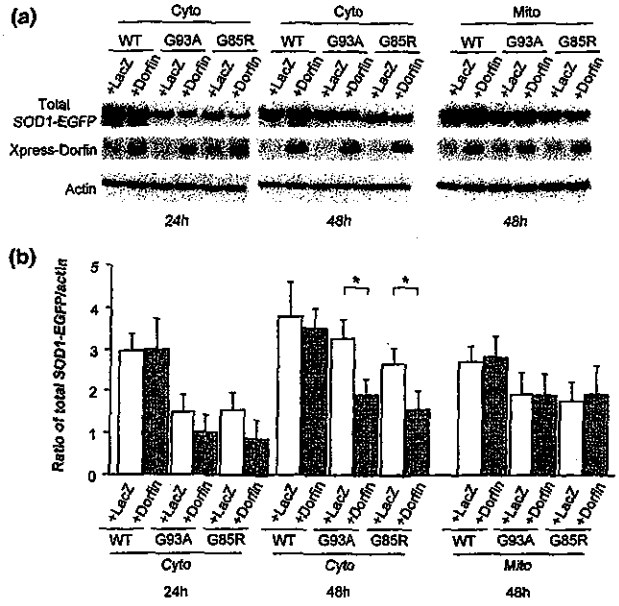

Fig. 2 Level of total SOD1-EGFP fusion protein. (a) Levels of total SOD1-EGFP fusion protein and Xpress-Dorfin fusion protein. (b) Densitometric analysis of total SOD1-EGFP fusion protein expressed as a ratio to actin. Dorfin significantly reduced the level of total SOD1-EGFP fusion protein expressed by Cyto-G93A or Cyto-G85R, whereas it did not reduce that expressed by Mito-SOD1. Values are mean ± SD ($n = 4$). *$p < 0.05$ (two-way ANOVA with Tukey–Kramer post-hoc test).

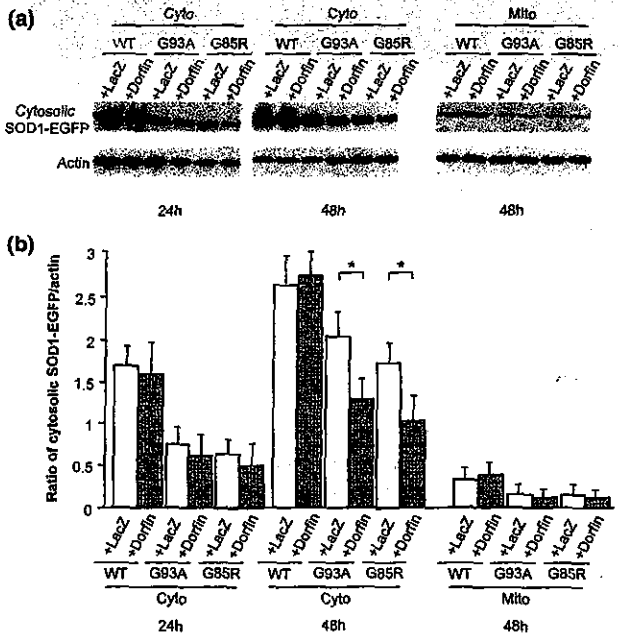

Fig. 3 Level of cytosolic SOD1-EGFP fusion protein. (a) Levels of cytosolic SOD1-EGFP fusion protein. (b) Densitometric analysis of cytosolic SOD1-EGFP fusion protein expressed as a ratio to actin. In the cytosolic fraction, Dorfin significantly reduced the levels of SOD1-EGFP fusion protein expressed by Cyto-G93A or Cyto-G85R. Mito-SOD1 showed very small amounts of SOD1-EGFP fusion proteins in the cytosolic fraction. Values are mean ± SD ($n = 4$). *$p < 0.05$ (two-way ANOVA with Tukey–Kramer post-hoc test).

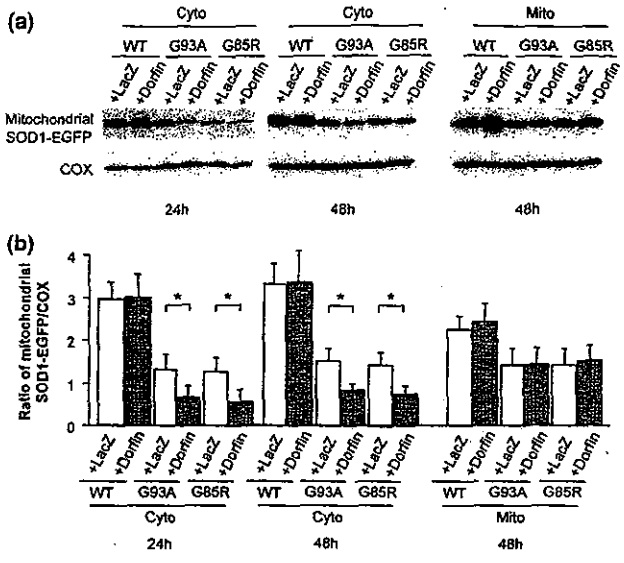

Fig. 4 Level of mitochondrial SOD1-EGFP fusion protein. (a) Levels of mitochondrial SOD1-EGFP fusion protein. (b) Densitometric analysis of mitochondrial SOD1-EGFP fusion protein expressed as a ratio to COX. In the mitochondrial fraction, Dorfin significantly reduced the level of SOD1-EGFP fusion protein expressed by Cyto-G93A or Cyto-G85R, whereas it did not reduce that expressed by Mito-SOD1. Values are mean ± SD ($n = 4$). *$p < 0.05$ (two-way ANOVA with Tukey–Kramer post-hoc test).

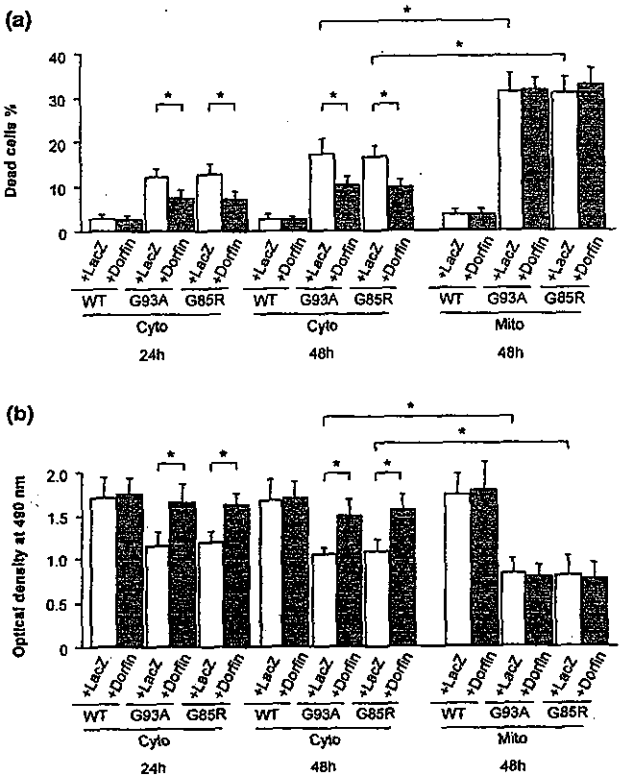

Fig. 5 (a) Frequency of dead cells and (b) mitochondrial impairment analyzed by MTS assay. The cells with Mito-G93A and Mito-G85R exhibited a significantly higher level of cell death and mitochondrial impairment than those with Cyto-G93A and Cyto-G85R. Dorfin significantly decreased cell death and mitochondrial impairment induced by Cyto-G93A and Cyto-G85R, whereas it did not affect those induced by Mito-SOD1. Values are mean ± SD ($n = 6$). *$p < 0.05$ (two-way ANOVA with Tukey–Kramer post-hoc test).

Dorfin protects neuronal cells from mutant SOD1-mediated neurotoxicity by reducing mitochondrial mutant SOD1

As we demonstrated previously (Takeuchi *et al.* 2002a), the cells with Cyto-G93A and Cyto-G85R underwent cell death (Fig. 5a) and mitochondrial impairment (Fig. 5b), whereas those with Cyto-WT did not. The cells with Mito-G93A and Mito-G85R exhibited significantly more cell death and mitochondrial impairment than those with Cyto-G93A and Cyto-G85R, whereas those with Mito-WT did not (Fig. 5). Co-expression of Dorfin significantly ameliorated cell death and mitochondrial impairment induced by Cyto-G93A and Cyto-G85R (Fig. 5), as in our previous report (Niwa *et al.* 2002). In contrast, Dorfin did not affect cell death and mitochondrial impairment induced by Mito-SOD1 (Fig. 5), whose protein level Dorfin did not reduce. These findings suggest that Dorfin ameliorates mutant SOD1-mediated neurotoxicity by reducing the accumulation of mutant SOD1 in the mitochondria.

Dorfin reduces mitochondrial cytochrome *c* release and sequential activation of caspase-9 and caspase-3

We next assessed whether Dorfin reduced the mitochondrial death signal associated with the mutant SOD1-mediated cytotoxicity. Western blots revealed that Cyto-G93A and Cyto-G85R induced a gradual increase in the cytochrome *c* released from the mitochondria into the cytosol, whereas Cyto-WT did not (Fig. 6). The cells with Mito-G93A and Mito-G85R also exhibited a higher level of cytochrome *c* release than those with Cyto-G93A and Cyto-G85R, whereas those with Mito-WT did not (Fig. 6). Co-expression of Dorfin significantly reduced the release of cytochrome *c* from the mitochondria into the cytosol induced by Cyto-G93A and Cyto-G85R (Fig. 6). In the cells with Mito-G93A and Mito-G85R, however, Dorfin did not reduce the cytochrome c release from the mitochondria into the cytosol (Fig. 6).

Next, we examined whether Dorfin affected the downstream signal cascade of the activation of caspase-9 and caspase-3 following the release of mitochondrial cytochrome *c*. As we demonstrated previously (Takeuchi *et al.* 2002a), western blots revealed that Cyto-G93A and Cyto-G85R induced gradual activation of caspase-9 and caspase-3, whereas Cyto-WT did not (Figs 7 and 8). The cells with Mito-G93A and Mito-G85R exhibited a higher level of activation of caspase-9 and caspase-3 than those with Cyto-G93A and Cyto-G85R, whereas those with Mito-WT did not (Figs 7 and 8). Co-expression of Dorfin significantly reduced

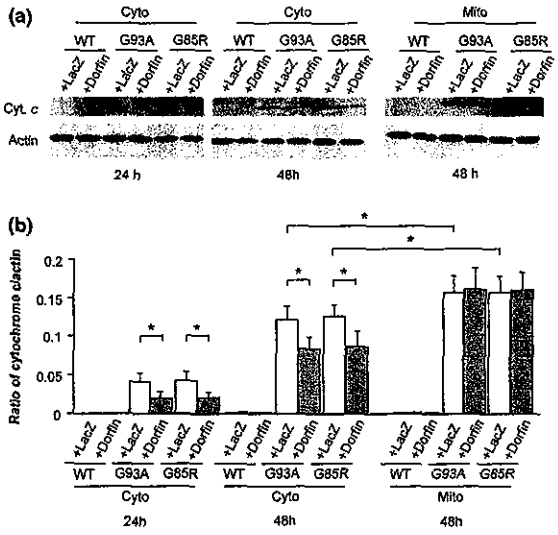

Fig. 6 Western blot analysis of cytochrome *c* release. (a) Time course of mitochondrial cytochrome *c* release into the cytosol. *(b) Densitometric* analysis of cytochrome *c* release expressed as a ratio to COX. *The cells with Mito-G93A and Mito-G85R exhibited significantly* more cytochrome *c* release than those with Cyto-G93A and Cyto-G85R. *Dorfin* significantly reduced the amount of mitochondrial cytochrome *c* released into the cytosol induced by Cyto-G93A and Cyto-G85R, whereas it did not affect that induced by Mito-SOD1. Values are mean ± SD ($n = 4$). *$p < 0.05$ (two-way ANOVA with Tukey–Kramer post-hoc test).

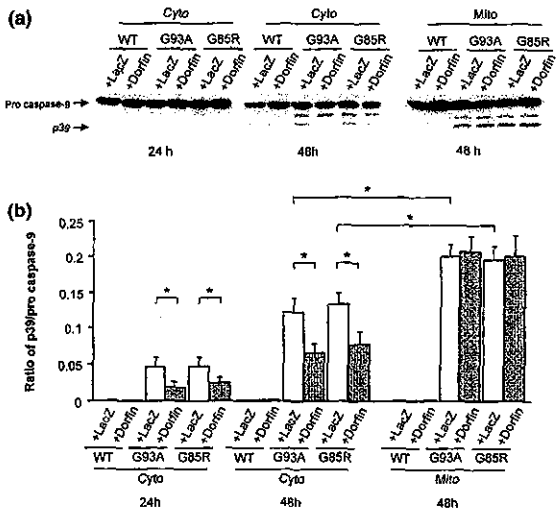

Fig. 7 Western blot analysis of caspase-9 activation. (a) Time course of the activation of caspase-9. (b) Densitometric analysis of caspase-9 activation. The cells with Mito-G93A and Mito-G85R exhibited significantly more activation of caspase-9 than those with Cyto-G93A and Cyto-G85R. *Dorfin significantly reduced* the activation of caspase-9 induced by Cyto-G93A and Cyto-G85R, whereas it did not reduce that induced by Mito-SOD1. Values are mean ± SD ($n = 4$). *$p < 0.05$ (two-way ANOVA with Tukey–Kramer post-hoc test).

the activation of caspase-9 and caspase-3 induced by Cyto-G93A and Cyto-G85R (Figs 7 and 8). However, Dorfin did not reduce the activation of caspase-9 and caspase-3 induced by Mito-G93A and Mito-G85R (Figs 7 and 8), as it did not reduce the release of cytochrome *c* induced by Mito-G93A and Mito-G85R (Fig. 6). These findings combined with the aforementioned observations suggest that the reduction in the amount of mitochondrial mutant SOD1 due to Dorfin results in attenuated activation of the mitochondrial PCD pathway and prevents eventual cell death.

Discussion

In the present study, we first demonstrated that Dorfin, an E3 for mutant SOD1s, attenuated the activation of the mitochondrial PCD pathway and prevented eventual cell death in a neuronal cell model of FALS by reducing the amount of mutant SOD1 in the mitochondria. Dorfin reduced the levels of both cytosolic and mitochondrial mutant SOD1-EGFP fusion proteins that were expressed by Cyto-G93A and Cyto-G85R without organelle-oriented signals, whereas Dorfin did not affect the level of mutant SOD1-EGFP fusion protein that was expressed by Mito-G93A and Mito-G85R with mitochondrial localizing signals. The reduction in the level of

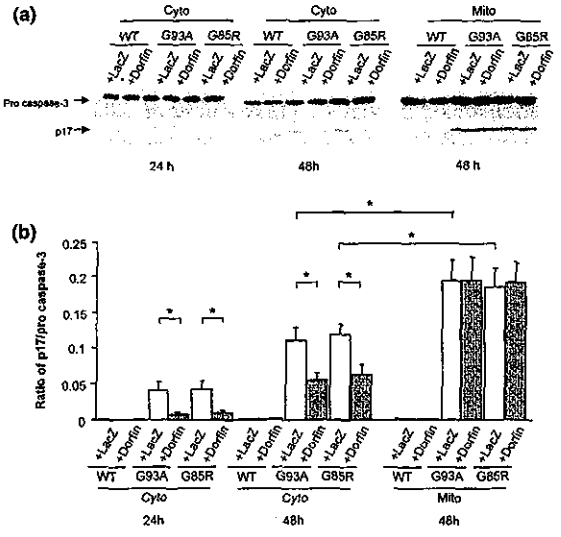

Fig. 8 Western blot analysis of caspase-3 activation. (a) Time course of activation of caspase-3. (b) Densitometric analysis of caspase-3 activation. The cells with Mito-G93A and Mito-G85R exhibited significantly more activation of caspase-3 than those with Cyto-G93A and Cyto-G85R. Dorfin significantly reduced the activation of caspase-3 induced by Cyto-G93A and Cyto-G85R, whereas it did not reduce that induced by Mito-SOD1. Values are mean ± SD ($n = 4$). *$p < 0.05$ (two-way ANOVA with Tukey–Kramer post-hoc test).

mitochondrial SOD1-EGFP was observed earlier than that of total or cytosolic SOD1-EGFP. Moreover, Dorfin was present in the cytosol, not in the mitochondria. These findings indicated that the mitochondrial mutant SOD1 without organelle-oriented signals (Cyto-G93A and Cyto-G85R) might be translocated from the cytosol, and we suggest that Dorfin reduces the mitochondrial accumulation of mutant SOD1 by enhancing the degradation of mutant SOD1 in the cytosol through the ubiquitin–proteasomal pathway, thereby reducing the uptake of mutant SOD1 into the mitochondria.

Many reports have documented mitochondrial involvement in ALS and FALS. Mitochondrial degeneration with vacuolization or membrane disintegration in motor neurons is one of the earliest pathological findings in FALS Tg mice (Dal Canto and Gurney 1994; Wong *et al.* 1995; Hirano 1996; Kong and Xu 1998; Jaarsma *et al.* 2000; Higgins *et al.* 2003). Moreover, mitochondrial dysfunction such as altered calcium homeostasis (Carrì *et al.* 1997; Menzies *et al.* 2002b), decreased respiratory chain complex activity (Mattiazzi *et al.* 2002; Menzies *et al.* 2002a), alteration of mitochondria-related gene expression (Yoshihara *et al.* 2002) and an increase in reactive oxygen species (Beretta *et al.* 2003) have been reported in *in vitro* and *in vivo* models of FALS. Several studies have documented that SOD1, which has been considered a cytosolic enzyme, also exists in the mitochondrial intermembrane space (Okado-Matsumoto and Fridovich 2001; Sturtz *et al.* 2001; Higgins *et al.* 2002) and that the mitochondrial vacuoles are lined with mutant SOD1 in a FALS Tg mice model (Jaarsma *et al.* 2001; Higgins *et al.* 2003). Although the mitochondria-oriented vector we used here is designed to localize proteins to the mitochondrial matrix, we predict that SOD1-EGFP also exists in the mitochondrial intermembrane space through the process of its uptake into the mitochondrial matrix in our model, although were not able to confirm this. Recent studies also revealed that SOD1 in the mitochondria originates from the uptake of SOD1 in the cytosol (Sturtz *et al.* 2001; Okado-Matsumoto and Fridovich 2002; Field *et al.* 2003). At least our result provided enough evidence that Dorfin interacts with mutant SOD1 in the cytosol, not in the mitochondria. Thus we suggest that Dorfin indirectly reduces the mitochondrial accumulation of mutant SOD1 by reducing the uptake of mutant SOD1 into the mitochondria.

Previous studies demonstrated that the mitochondrial PCD pathway, cytochrome *c* release and subsequent caspase activation, might contribute to the motor neuron cell death in FALS (Durham *et al.* 1997; Martin 1999; Li *et al.* 2000; Pasinelli *et al.* 2000; Guégan *et al.* 2001; Kriz *et al.* 2002; Zhu *et al.* 2002). Thus, inhibiting the activation of the mitochondrial PCD pathway is potentially useful in the treatment of FALS. Methods for this include inhibition of cytochrome c release by minocycline (Zhu *et al.* 2002; Kriz *et al.* 2002), co-expression of bcl-2 (Lee *et al.* 2001) or X-chromosome-linked inhibitor of apoptosis protein (Ishigaki *et al.* 2002), and treatment with a broad caspase inhibitor zVAD-fmk (Pasinelli *et al.* 2000; Takeuchi *et al.* 2002a) or a caspase-9 specific inhibitor zLEHD-fmk (Takeuchi *et al.* 2002a). In this study, we demonstrated that Dorfin reduces the amount of mitochondrial mutant SOD1, attenuates the activation of the mitochondrial PCD pathway and prevents eventual neuronal cell death. It is therefore possible that reducing the amount of mutant SOD1 in the mitochondria may be adopted as a new therapeutic strategy for mutant SOD1-associated FALS.

Recent studies have suggested that some E3s, including Dorfin, act in a quality-control system to degrade cytosolic or transmembranous unfolded abnormal proteins (Moynihan *et al.* 1999; Fang *et al.* 2001; Meacham *et al.* 2001; Murata *et al.* 2001; Yoshida *et al.* 2002). The mitochondria also have a quality-control system that depends on mitochondria-specific molecular chaperones and ATPases associated with diverse cellular activities (AAA) proteases such as chaperonin 60 (Gottesman *et al.* 1997), mitochondrial heat-shock protein 70 (Savel'ev *et al.* 1998), and homologs of Lon, Yme1p, ClpP and ClpX (Wang *et al.* 1993; Suzuki *et al.* 1997; Langer 2000; Shah *et al.* 2000; Kang *et al.* 2002; Röttgers *et al.* 2003). A recent study documented that the accumulation of unfolded abnormal proteins in the mitochondria itself up-regulated the nuclear gene expression encoding mitochondrial-specific molecular chaperones (Zhao *et al.* 2002). Even though the mitochondria are able to dispose of abnormal proteins, they appear to have limited capacity to do this. They also seem to release death signals when abnormal proteins overflow their disposing capacity. Combination therapy such as Dorfin and mitochondria-specific molecular chaperones or AAA proteases thus seems more effective. Further investigations are needed to develop this therapeutic avenue.

There remains the problem of how the mutant SOD1 induces the mitochondrial PCD pathway. One of our previous studies revealed that bcl-2 family pro-apoptotic proteins, such as Bax, Bak, Bid, Bad and Bim, and other mitochondrial death signals such as apoptosis-inducing factor (AIF) and second mitochondria-derived activator of caspase (Smac) were not involved in the neuronal cell death in our model (Takeuchi *et al.* 2002a). Other studies have reported that translocation of Bax and cleavage of Bid were associated with neuronal cell death in the FALS Tg mouse model (Guégan *et al.* 2001; 2002), but there is a possibility that the surrounding environment of motor neurons such as astrocytes, microglia or dying neurons might have been affected in these models. Moreover, we have indicated that a non-apoptotic form of PCD might contribute to neuronal cell death through the mitochondrial PCD pathway in our model (Takeuchi *et al.* 2002a). Another report also mentioned that a non-apoptotic type of PCD acting through the mitochondrial PCD pathway might underlie mutant SOD1-related neurotoxicity (Guégan and Przedborski 2003). Further *in vivo*

investigations are needed to shed light on the mechanism of mutant SOD1-mediated neuronal cell death.

In this study we demonstrated that Dorfin, an E3 for mutant SOD1s, significantly reduced the level of mutant SOD1 in the mitochondria, attenuated the subsequent activation of the mitochondrial PCD pathway and prevented eventual neuronal cell death in a neuronal cell model of FALS. Reducing the accumulation of mutant SOD1 in the mitochondria may have an important place in the therapeutic strategy for mutant SOD1-associated FALS, and Dorfin may play a key role in this.

Acknowledgements

We are grateful to Dr Keiji Tanaka (Department of Molecular Oncology, The Tokyo Metropolitan Institute of Medical Science) for his helpful comments. This work was supported by grants from the Ministry of Health, Labor and Welfare of Japan, and a Center of Excellence grant from the Ministry of Education, Culture, Sports, Science and Technology of Japan.

References

Ardley H. C., Tan N. G. S., Rose S. A., Markham A. F. and Robinson P. A. (2001) Features of the Parkin/Ariadne-like ubiquitin ligase, HHARI, that regulate its interaction with the ubiquitin-conjugating enzyme, UbcH7. *J. Biol. Chem.* **276**, 19640–19647.

Beretta S., Sala G., Mattavelli L., Ceresa C., Casciati A., Ferri A., Carr i M. T. and Ferrarese C. (2003) Mitochondrial dysfunction due to mutant copper/zinc superoxide dismutase associated with amyotrophic lateral sclerosis is reversed by *N*-acetylcysteine. *Neurobiol. Dis.* **13**, 213–221.

Carri M. T., Ferri A., Battistoni A., Famhy L., Gabbianelli R., Poccia F. and Rotilio G. (1997) Expression of a Cu,Zn superoxide dismutase typical of familial amyotrophic lateral sclerosis induces mitochondrial alteration and increase of cytosolic Ca^{2+} concentration in transfected neuroblastoma SH-SY5Y cells. *FEBS Lett.* **414**, 365–368.

Dal Canto M. C. and Gurney M. E. (1994) Development of central nervous system pathology in a murine transgenic model of human amyotrophic lateral sclerosis. *Am. J. Pathol.* **145**, 1271–1279.

Durham H. D., Roy J., Dong L. and Figlewic Z. D. A. (1997) Aggregation of mutant Cu/Zn superoxide dismutase proteins in a culture model of ALS. *J. Neuropathol. Exp. Neurol.* **56**, 523–530.

Fang S., Ferrone M., Yang C., Jensen J. P., Tiwari S. and Weissman A. M. (2001) The tumor autocrine motility factor receptor, gp78, is a ubiquitin protein ligase implicated in degradation from the endoplasmic reticulum. *Proc. Natl Acad. Sci. USA* **98**, 14422–14427.

Field L. S., Furukawa Y., O'Halloran T. V. and Culotta V. C. (2003) Factors controlling the uptake of yeast Cu/Zn superoxide dismutase into mitochondria. *J. Biol. Chem.* **278**, 28052–28059.

Gottesman S., Wickner S. and Maurizi M. R. (1997) Protein quality control: triage by chaperones and proteases. *Genes Dev.* **11**, 815–823.

Guégan C. and Przedborski S. (2003) Programmed cell death in amyotrophic lateral sclerosis. *J. Clin. Invest.* **111**, 153–161.

Guégan C., Vila M., Rosoklija G., Hays A. P. and Przedborski S. (2001) Recruitment of the mitochondrial-dependent apoptotic pathway in amyotrophic lateral sclerosis. *J. Neurosci.* **21**, 6569–6576.

Guégan C., Vila M., Teissman P., Chen C., Onténiente B., Li M., Friedlander R. M. and Przedborski S. (2002) Instrumental activation of Bid by caspase-1 in a transgenic mouse model of ALS. *Mol. Cell. Neurosci.* **20**, 553–562.

Higgins C. M., Jung C., Ding H. and Xu Z. (2002) Mutant Cu,Zn superoxide dismutase that causes motoneuron degeneration is present in mitochondria in the CNS. *J. Neurosci.* **22 RC215.**

Higgins C. M. J., Jung C. and Xu Z. (2003) ALS-associated mutant SOD1G93A causes mitochondrial vacuolation by expansion of the intermembrane space and by involvement of SOD1 aggregation and peroxisomes. *BMC Neurosci.* **4**, 16–29.

Hirano A. (1996) Neuropathology of ALS: an overview. *Neurology* **47**, S63–S66.

Ishigaki S., Liang Y., Yamamoto M., Niwa J., Ando Y., Yoshihara T., Takeuchi H., Doyu M. and Sobue G. (2002) X-linked inhibitor of apoptosis protein is involved in mutant SOD1-mediated neuronal degeneration. *J. Neurochem.* **82**, 576–584.

Jaarsma D., Haasdijk E. D., Grashorn J. A. C., Hawkins R., van Duijn W., Verspaget H. W., London J. and Holstege J. C. (2000) Human Cu/Zn superoxide dismutase (SOD1) overexpression in mice causes mitochondrial vacuolization, axonal degeneration, and premature motoneuron death and accelerates motoneuron disease in mice expressing a familial amyotrophic lateral sclerosis mutant SOD1. *Neurobiol. Dis.* **7**, 623–643.

Jaarsma D., Rognoni F., van Duijn W., Verspaget H. W., Haasdijk E. D. and Holstege J. C. (2001) CuZn superoxide dismutase (SOD1) accumulates in vacuolated mitochondria in transgenic mice expressing amyotrophic lateral sclerosis-linked SOD1 mutations. *Acta Neuropathol.* **102**, 293–305.

Kang S. G., Ortega J., Singh S. K., Wang N., Huang N., Steven A. C. and Maurizi M. R. (2002) Functional proteolytic complexes of the human mitochondrial ATP-dependent protease, hClpXP. *J. Biol. Chem.* **277**, 21095–21102.

Kong J. and Xu Z. (1998) Massive mitochondrial degeneration in motor neurons triggers the onset of amyotrophic lateral sclerosis in mice expressing a mutant SOD1. *J. Neurosci.* **18**, 3241–3250.

Kriz J., Nguyen M. D. and Julien J. P. (2002) Minocycline slows disease progression in a mouse model of amyotrophic lateral sclerosis. *Neurobiol. Dis.* **10**, 268–278.

Langer T. (2000) AAA proteases: cellular machines for degrading membrane proteins. *Trends Biochem. Sci.* **25**, 247–251.

Lee M. H., Hyun D.-H., Halliwell B. and Jenner P. (2001) Effect of overexpression of wild-type and mutant Cu/Zn-superoxide dismutases on oxidative stress and cell death induced by hydrogen peroxide, 4-hydroxynonenal or serum deprivation: potentiation of injury by ALS-related mutant superoxide dismutases and protection by Bcl-2. *J. Neurochem.* **78**, 209–220.

Li M., Ona V. O., Guégan C. *et al.* (2000) Functional role of caspase-1 and caspase-3 in an ALS transgenic mouse model. *Science* **288**, 335–339.

Martin L. J. (1999) Neuronal death in amyotrophic lateral sclerosis is apoptosis: possible contribution of a programmed cell death mechanism. *J. Neuropathol. Exp. Neurol.* **58**, 459–471.

Mattiazzi M., D'Aurelio M., Gajewski C. D., Martushova K., Kiaei M., Beal M. F. and Manfredi G. (2002) Mutated human SOD1 causes dysfunction of oxidative phosphorylation in mitochondria of transgenic mice. *J. Biol. Chem.* **277**, 29626–29633.

Meacham G. C., Patterson C., Zhang W., Younger J. M. and Cyr D. M. (2001) The Hsc70 co-chaperone CHIP targets immature CFTR for proteasomal degradation. *Nat. Cell Biol.* **3**, 100–105.

Menzies F. M., Cookson M. R., Taylor R. W., Turnbull D. M., Chrzanowska-Lightowlers Z. M., Dong L., Figlewicz D. A. and Shaw P. J. (2002a) Mitochondrial dysfunction in a cell culture model of familial amyotrophic lateral sclerosis. *Brain* **125**, 1522–1533.

Menzies F. M., Ince P. G. and Shaw P. J. (2002b) Mitochondrial involvement in amyotrophic lateral sclerosis. *Neurochem. Int.* **40**, 543–551.

Moynihan T. P., Ardley H. C., Nuber U., Rose S. A., Jones P. F., Markham A. F., Scheffner M. and Robinson P. A. (1999) The ubiquitin-conjugating enzymes UbcH7 and UbcH8 interact with RING finger/IBR motif-containing domains of HHARI and H7-AP1. *J. Biol. Chem.* **274**, 30963–30968.

Murata S., Minami Y., Minami M., Chiba T. and Tanaka K. (2001) CHIP is a chaperone-dependent E3 ligase that ubiquitylates unfolded protein. *EMBO Report* **2**, 1133–1138.

Niwa J., Ishigaki S., Doyu M., Suzuki T., Tanaka K. and Sobue G. (2001) A novel centrisomal RING-finger protein, Dorfin, mediates ubiquitin ligase activity. *Biochem. Biophys. Res. Commun.* **281**, 706–713.

Niwa J., Ishigaki S., Hishikawa N., Yamamoto M., Doyu M., Murata S., Tanaka K., Taniguchi N. and Sobue G. (2002) Dorfin ubiquitylates mutant SOD1 and prevents mutant SOD1-mediated neurotoxicity. *J. Biol. Chem.* **277**, 36793–36798.

Okado-Matsumoto A. and Fridovich I. (2001) Subcellular distribution of superoxide dismutase (SOD) in rat liver. *J. Biol. Chem.* **276**, 38388–38393.

Okado-Matsumoto A. and Fridovich I. (2002) Amyotrophic lateral sclerosis: a proposed mechanism. *Proc. Natl Acad. Sci. USA* **99**, 9010–9014.

Pasinelli P., Houseweart M. K., Brown R. H. Jr and Cleveland D. W. (2000) Caspse-1 and -3 are sequentially activated in motor neuron death in Cu,Zn superoxide dismutase-mediated familial amyotrophic lateral sclerosis. *Proc. Natl Acad. Sci. USA* **97**, 13901–13906.

Raoul C., Estévez A. G., Nishimune H., Cleveland D. W., deLapeyrière O., Henderson C. E., Haase G. and Pettmann B. (2002) Motoneuron death triggered by a specific pathway downstream of Fas; potentiation by ALS-linked SOD1 mutations. *Neuron* **35**, 1067–1083.

Rosen D. R., Siddique T., Patterson D. *et al.* (1993) Mutations in Cu/Zn superoxide dismutase gene are associated with familial amyotrophic lateral sclerosis. *Nature* **362**, 59–62.

Röttgers K., Zufall N., Guiard B. and Voos W. (2003) The ClpB homolog Hsp78 is required for the efficient degradation of proteins in the mitochondrial matrix. *J. Biol. Chem.* **277**, 45829–45837.

Savel'ev A. S., Novikova L. A., Kovaleva I. E., Luzikov V. N., Neupert W. and Langer T. (1998) ATP-dependent proteolysis in mitochondria. *J. Biol. Chem.* **273**, 20596–20602.

Shah Z. H., Hakkaart G. A. J., Arku B., de Jong L., van der Spek H., Grivell L. A. and Jacobs H. T. (2000) The human homologue of the yeast mitochondrial AAA metalloprotease Yme1p complements a yeast *yme1* disruptant. *FEBS Lett.* **478**, 267–270.

Sturtz L. A., Diekert K., Jensen L. T., Lill R. and Culotta V. C. (2001) A fraction of yeast Cu,Zn-superoxide dismutase and its metallochaperone, CCS, localize to the intermembrane space of mitochondria. *J. Biol. Chem.* **276**, 38084–38089.

Suzuki C. K., Rep M., van Dijl J. M., Suda K., Grivell L. A. and Schatz G. (1997) ATP-dependent proteases that also chaperone protein biogenesis. *Trends Biochem. Sci.* **22**, 118–123.

Takeuchi H., Kobayashi Y., Ishigaki S., Doyu N. and Sobue G. (2002a) Mitochondrial localization of mutant superoxide dismutase 1 triggers caspase-dependent cell death in a cellular model of familial amyotrophic lateral sclerosis. *J. Biol. Chem.* **277**, 50966–50972.

Takeuchi H., Kobayashi Y., Yoshihara T., Niwa J., Doyu M., Ohtsuka K. and Sobue G. (2002b) Hsp70 and Hsp40 improve neurite outgrowth and suppress intracytoplasmic aggregate formation in cultured neuronal cells expressing mutant SOD1. *Brain Res.* **949**, 11–22.

Wang N., Gottesman S., Willingham M. C., Gottesman M. M. and Maurizi M. R. (1993) A human mitochondrial ATP-dependent protease that is highly homologous to bacterial Lon protease. *Proc. Natl Acad. Sci. USA* **90**, 11247–11251.

Wong P. C., Pardo C. A., Borchelt D. R., Lee M. K., Copeland N. G., Jenkins N. A., Sisodia S. S., Cleveland D. W. and Price D. L. (1995) An adverse property of a familial ALS-linked SOD1 mutation causes motor neuron disease characterized by vacuolar degeneration of mitochondria. *Neuron* **14**, 1105–1116.

Yim M. B., Kang J. H., Yim H. S., Kwak H. S., Chock P. B. and Stadtman E. R. (1996) A gain-of-function of an amyotrophic lateral sclerosis-associated Cu,Zn-superoxide dismutase mutant: an enhancement of free radical formation due to a decrease in K_m for hydrogen peroxide. *Proc. Natl Acad. Sci. USA* **93**, 5709–5714.

Yoshida Y., Chiba T., Tokunaga F. *et al.* (2002) E3 ubiquitin ligase that recognizes sugar chains. *Nature* **418**, 438–442.

Yoshihara T., Ishigaki S., Yamamoto M., Liang Y., Niwa J., Takeuchi H., Doyu M. and Sobue G. (2002) Differential expression of inflammation- and apoptosis-related genes in spinal cords of a mutant SOD1 transgenic mouse model of familial lateral sclerosis. *J. Neurochem.* **80**, 158–167.

Zhao Q., Wang J., Levichkin I. V., Stasinopoulos S., Ryan M. T. and Hoogenraad N. J. (2002) A mitochondrial specific stress response in mammalian cells. *EMBO J.* **21**, 4411–4419.

Zhu S., Stavrovskaya I. G., Drozda M. *et al.* (2002) Minocycline inhibits cytochrome *c* release and delays progression of amyotrophic lateral sclerosis. *Nature* **417**, 74–78.

Pathology of early- vs late-onset TTR Met30 familial amyloid polyneuropathy

H. Koike, MD, PhD; K. Misu, MD, PhD; M. Sugiura, MD; M. Iijima, MD; K. Mori, MD, PhD; M. Yamamoto, MD, PhD; N. Hattori, MD, PhD; E. Mukai, MD, PhD; Y. Ando, MD, PhD; S. Ikeda, MD, PhD; and G. Sobue, MD, PhD

Abstract—*Background:* Late-onset type I familial amyloid polyneuropathy (FAP TTR Met30) cases unrelated to endemic foci in Japan show clinical features setting them apart from early-onset cases in endemic foci. *Objective:* To compare pathologic features between the early- and late-onset types. *Methods:* Pathologic findings in FAP TTR Met30 with onset before age 50 in relation to endemic foci (11 cases) were compared with those in 11 later-onset cases unrelated to endemic foci. *Results:* Sural nerve biopsy specimens showed predominantly small-fiber loss in early-onset cases; variable fiber size distribution, axonal sprouting, and relatively preserved unmyelinated fibers characterized late-onset cases. Autopsy cases representing both groups showed amyloid deposition throughout the length of nerves and in sympathetic and sensory ganglia, but amounts were greater in early-onset cases. Amyloid deposition and neuronal cell loss were greater in sympathetic than dorsal root ganglia in early-onset cases; the opposite was true in late-onset cases. Size assessment of remaining neurons in these ganglia suggested predominant loss of small neurons in early-onset cases but loss of neurons of all sizes in late-onset cases. Transthyretin-positive, Congo red-negative amorphous material was more conspicuous in nerves from late- than early-onset cases. In extraneural sites, amyloid was more conspicuous in thyroid and kidney from early-onset cases and in heart and hypophysis from late-onset cases. In early-onset cases, cardiac amyloid deposition was prominent in the atrium and subendocardium but was conspicuous throughout the myocardium in late-onset cases. *Conclusion:* The pathology of early- and late-onset FAP TTR Met30 correlated well with differences in clinical findings.

NEUROLOGY 2004;63:129–138

Familial amyloid polyneuropathy type I (transthyretin Met30-associated familial amyloid polyneuropathy; FAP TTR Met30), in which methionine is substituted for valine at position 30 of transthyretin, is the most common type of FAP in Japan as well as in Western countries.[1-6] In Japan, cases have been particularly concentrated in two geographic areas: the village of Ogawa in Nagano Prefecture on the island of Honshu and the city of Arao in Kumamoto Prefecture on the island of Kyushu.[3,4] Although there are exceptions, typical cases of FAP TTR Met30 in these two endemic foci are characterized by early age at onset (second or third decade), a high penetrance rate, marked autonomic dysfunction, selective loss of superficial sensation including nociception and thermal sensation, atrioventricular conduction block requiring pacemaker implantation, steady progression of disease over 10 to 15 years, and presence of anticipation concerning age at onset.[3,4,7-11]

In contrast to these early-onset FAP TTR Met30 cases in endemic foci, we have reported the presence of a late-onset type of FAP TTR Met30 in a wide distribution throughout Japan.[9,10,12] Features of these cases were distinct from those of early-onset cases related to endemic foci. These differences included onset at ages over 50 years, a low penetrance rate, relatively mild autonomic dysfunction, loss of all sensory modalities rather than sensory dissociation, frequent presence of cardiomegaly, extreme male preponderance, and absence of anticipation concerning age at onset.[9,10,12] These geographic and clinical differences were confirmed in a subsequent nationwide survey.[11] Similar geographic and clinical contrasts between early- and late-onset types of FAP TTR Met30 have been reported in Portugal,[1,5,13] although not in the form of a large-scale comparative study.

The reasons for contrasting features in early- and late-onset FAP with the same mutation in the transthyretin gene have not yet been determined. In the current study, we investigated pathologic features of Japanese patients with early- and late-onset FAP TTR Met30, seeking explanations for the clinical differences.

Patients and methods. Pathologic findings were compared between consecutive patients with early- and late-onset FAP TTR Met30 who attended the Nagoya University Graduate School of Medicine for sural nerve biopsy or autopsy from 1989 to 2003. Inclusion criteria for early-onset cases were FAP TTR Met30 with an onset age under 50 years and a relationship to one of the two Japanese endemic foci within the two most recent prior genera-

From the Department of Neurology (Drs. Koike, Misu, Sugiura, Iijima, Mori, Yamamoto, Hattori, and Sobue), Nagoya University Graduate School of Medicine, Department of Neurology (Dr. Mukai), Nagoya National Hospital, Department of Laboratory Medicine (Dr. Ando), Kumamoto University School of Medicine, and Third Department of Medicine (Dr. Ikeda), Shinshu University School of Medicine, Matsumoto, Japan.

Supported by grants from the Ministry of Health, Labor, and Welfare of Japan.

Received October 8, 2003. Accepted in final form February 23, 2004.

Address correspondence and reprint requests to Dr. G. Sobue, Department of Neurology, Nagoya University Graduate School of Medicine, Nagoya 466-8550, Japan; e-mail: sobueg@med.nagoya-u.ac.jp

Table 1 Background and clinical features of early- and late-onset FAP TTR Met30

Case no.	Sex	Age at onset/ death, y	Duration of illness until biopsy, y	Relationship to endemic foci	Family history	Initial symptom	Sensory dissociation	Cardiac involvement		Cause of death
								Cardiomegaly	Pacemaker implantation	
Early-onset group										
1	F	28/35	—	+	+	A	+	−	+	Sudden death
2	F	37/51	—	+	+	A	+	−	+	Pneumonia
3	M	24/41	3	+	+	A	+	−	−	Pneumonia
4	M	35	2.5	+	ND*	W	+	−	−	
5	F	33	6	+	+	P	−	−	+	
6	M	35	3	+	+	P	+	+	−	
7	M	36	2	+	+	A	+	−	−	
8	M	40	1	+	+	P	+	−	−	
9	M	28	1	+	+	P	+	−	−	
10	F	34	2	+	ND*	A	+	−	+	
11	F	41	3	+	+	A	−	−	+	
Late-onset group										
12	M	64/67	2	−	−	P	+	−	−	Lung cancer
13	M	62/68	3	−	−	P	+	+	−	Heart failure
14	M	52/62	3	−	−	P	−	+	−	Heart failure
15	M	67	2	−	+	P	−	−	−	
16	M	77	0.5	−	−	P, HF	−	+	−	
17	M	56	1	−	−	W	−	+	−	
18	M	61	3	−	−	P	−	+	−	
19	M	56	3	−	−	P	−	+	−	
20	M	58	0.6	−	−	P	−	+	−	
21	M	60	1.25	−	−	A	−	+	−	
22	M	61	5	−	−	P, W	−	−	−	

Cardiomegaly was assessed at the time of first referral to the hospital. No patient belonged to the same kindred as another.

* Fathers of Cases 4 and 10 were from Ogawa Village but died of nonneurologic disease when the patients were children. Statistical significance (early-vs late-onset group) was present in the items of sex ($p < 0.05$), age at onset ($p < 0.0001$), relationship to endemic foci ($p < 0.0001$), family history ($p < 0.0001$), sensory dissociation ($p < 0.01$), cardiomegaly ($p < 0.01$), and pacemaker implantation ($p < 0.05$). Statistical analyses were performed using the χ^2 test or the Mann–Whitney U test as appropriate.

FAP = familial amyloid polyneuropathy; + = present; − = absent; A = autonomic symptoms; W = weakness in the lower legs; P = paresthesia in the legs; HF = heart failure; ND = not determined.

tions. For late-onset cases, inclusion criteria were FAP TTR Met30 with an onset age over 50 years and no relationship to the endemic foci within the two most recent prior generations. To confirm the diagnosis of FAP TTR Met30, DNA analyses for mutation of the transthyretin gene were performed in all patients as described previously.[4,14,15] Informed consent was obtained, and all aspects of the study were approved by the Ethics Committee of Nagoya University Graduate School of Medicine.

Of the 22 patients included, 11 were in the early-onset group and the other 11 belonged to the late-onset group (table 1). No patient in the study belonged to the same kindred as another. Age at onset in the early-onset group was 33.9 ± 5.4 years and in the late-onset group 61.3 ± 6.7 years. Duration from onset of neuropathy to sural nerve biopsy was 2.6 ± 1.5 years in the early-onset group and 2.2 ± 1.4 years in the late-onset group (no significant difference). Duration from onset to death in autopsy cases was 12.7 ± 5.1 years for early-onset disease but only 6.3 ± 3.5 years in late-onset cases. Clinical features in the two groups of patients agreed well with previous descriptions.[3,9,11] In the early-onset group, half of the patients initially had autonomic symptoms, and most patients manifested more profound impairment of superficial than deep sensation (i.e., sensory dissociation). Pacemaker implantation was required in five patients, and the apparent cause of death in one case was sudden cardiac arrest. In the late-onset group, on the other hand, most patients initially manifested paresthesias or weakness in the legs rather than autonomic symptoms. Sensory dissociation was infrequent, and most patients manifested cardiac hypertrophy evident by chest radiography or echocardiography as opposed to atrioventricular conduction block in the early-onset group.

Sural nerve biopsy was performed in nine of the early-onset cases and all of the late-onset cases as described previously.[16-19] Specimens were divided into two portions. The first was fixed in 2.5% glutaraldehyde in 0.125 *M* cacodylate buffer (pH 7.4). Most of this part was embedded in epoxy resin for morphometric and ultrastructural study. Density of myelinated fibers was assessed in toluidine blue-stained semithin sections using a computer-assisted image analyzer (Luzex FS; Nikon, Tokyo, Japan); densities of small and large myelinated fibers were calculated as described previously.[17-19] Clusters of two or more small myelinated fibers enclosed by one basement membrane were considered an instance of axonal sprouting.[20-22] For electron microscopic study,

Table 2 Pathologic findings in sural nerve biopsy specimens

Case no.	MF density, no./mm²				Axonal sprouting of MF, no./mm²	UMF density, no./mm²	Segmental de/remyelination, %	Axonal degeneration, %	Amyloid deposition, %
	Large	Small	Total	Small/large					
Early onset									
3	0	0	0	—*	0	0	ND†	ND†	ND
4	13	13	26	—*	0	0	ND†	ND†	7
5	11	22	33	—*	0	216	8	25	1
6	23	0	23	—*	0	212	ND†	ND†	2
7	711	395	1,106	0.56	0	431	5	21	1
8	2,700	1,449	4,149	0.54	9	2,370	10	17	0+
9	2,015	1,515	3,530	0.75	18	3,663	6	26	0+
10	1,090	427	1,517	0.39	6	844	3	9	4
11	1,659	237	1,896	0.14	10	861	ND	ND	0+
Mean ± SD	914 ± 1,018	451 ± 608	1,364 ± 1,583	0.48 ± 0.23	5 ± 7	993 ± 1,305	6.4 ± 2.7	19.6 ± 6.9	
Controls, n = 3	3,495 ± 179	5,172 ± 528	8,666 ± 665	1.48 ± 0.11		30,104 ± 1,115	3.7 ± 5.5	0.4 ± 0.3	
Late onset									
12	79	487	566	6.16	79	2,370	17	20	0+
13	619	527	1,146	0.85	40	7,973	1	37	0
14	329	1,172	1,501	3.56	184	10,990	8	14	0+
15	66	13	79	—*	0	1,293	19	25	1
16	92	250	342	3.30	53	2,155	2	15	0+
17	461	1,831	2,292	3.97	250	7,111	13	27	1
18	0	2,423	2,423	—*	224	4,310	6	19	0
19	132	132	264	1.00	13	2,586	6	24	0+
20	514	355	869	0.69	26	1,795	4	37	0
21	1,304	1,212	2,516	0.93	105	14,438	6	26	0
22	66	277	343	4.20	40	431	ND†	ND†	1
Mean ± SD	333 ± 386	789 ± 776	1,122 ± 925	2.74 ± 1.95	92 ± 88	7,308 ± 5,417	8.2 ± 6.1	24.4 ± 8.0	
Controls, n = 4	2,891 ± 251	4,995 ± 333	7,886 ± 334	1.74 ± 0.22		29,748 ± 3,587	9.5 ± 6.2	1.9 ± 1.9	

Control values for each group were age matched. Statistical significance (early-vs late-onset group) was present in the items of small/large ($p < 0.05$), axonal sprouting of MF ($p < 0.01$), and UMF density ($p < 0.01$). Statistical analyses were performed using the Mann–Whitney *U* test.

* Populations of myelinated fibers were too small to determine the ratio.
† Teased fibers could not be obtained owing to depletion of myelinated fibers.

MF = myelinated fiber; UMF = unmyelinated fiber; ND = not determined; 0+ = <0.5%.

epoxy resin-embedded specimens were cut into ultrathin transverse sections and stained with uranyl acetate and lead citrate. To assess the density of unmyelinated fibers, electron microscopic photographs were taken at a magnification of 4,000× in a random fashion to cover the area of ultrathin sections as described previously.[17,19,21] Density of unmyelinated fibers was estimated from these electron micrographs. The remainder of the glutaraldehyde-fixed sample was processed for teased fiber study, in which microscopic observations were classified according to criteria described previously.[17,18,23,24] The second portion of the specimen was fixed in 10% formalin solution and embedded in paraffin. Sections were cut by routine methods and stained with hematoxylin and eosin, Congo red, the Klüver–Barrera method, and the Masson trichrome method. Seven sural nerve specimens were obtained from subjects with nonneurologic diseases at autopsy and examined in the same manner as age-matched control subjects (three cases for early-onset group, age 39.0 ± 7.8 years; four cases for late-onset group, age 62.3 ± 7.9 years).

Autopsy was performed in three early-onset cases and three late-onset cases. The nervous system including brain, spinal cord, ventral and dorsal roots, dorsal root ganglia from L3 to L5, and sympathetic ganglia was removed, as were the visceral organs. Tissues were fixed in 10% formalin solution, embedded in paraffin, cut, and stained as described for sural nerve specimens. In two of the early-onset and one of the late-onset cases, the median nerve from the axilla to the wrist and the sciatic/tibial nerve from the upper thigh to above the medial malleolus also were removed and fixed in 0.05 *M* phosphate buffer (pH 7.4) containing 1.5% glutaraldehyde and 3% formalin. After fixation, samples were taken every 4 cm along the nerves, embedded in paraffin or epoxy resin, cut, and stained as described for sural nerve specimens. Portions of the ventral and dorsal spinal roots were also fixed and processed in the same manner. Some of the quantitative aspects of the peripheral nervous system findings in Cases 2 and 3 were previously published.[18] Some descriptive pathologic findings in the peripheral nervous system in Cases 12 to 14 also were roughly described previously.[9]

Numbers and diameters of sympathetic ganglion neurons and

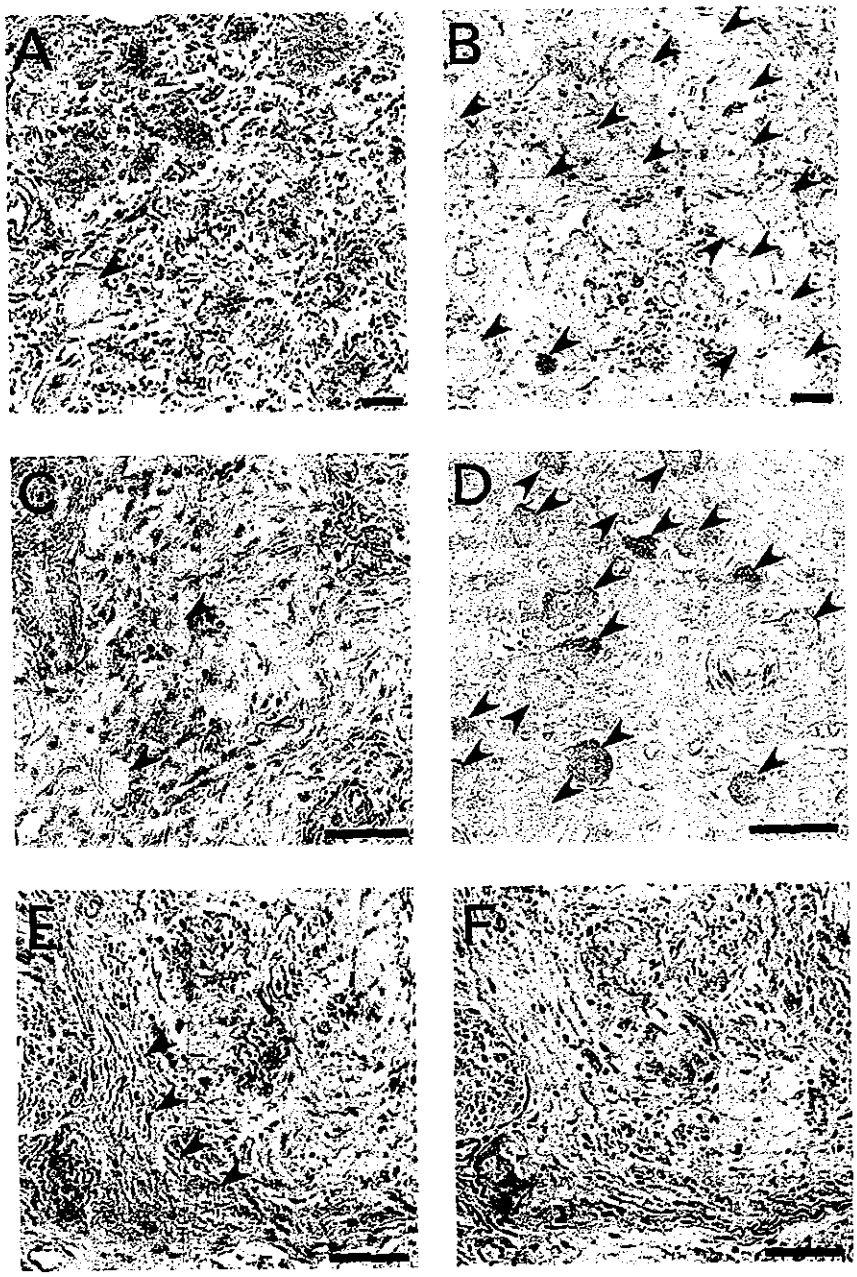

Figure 1. Representative postmortem findings in the peripheral nervous system. Amyloid deposits are identified by anti-human transthyretin antibody (A to E) or Congo red (F). (A, B) Dorsal root ganglia from early- and late-onset cases, respectively. (C, D) Sympathetic ganglia from early- and late-onset cases, respectively. In the dorsal root ganglia and sympathetic ganglia, amyloid deposition and neuronal cell loss are conspicuous in early-onset cases (A and C), whereas these are less severe in late-onset cases (B and D). Arrowheads indicate remaining neurons. (E, F) Consecutive specimens of the proximal part of sciatic nerve from a late-onset case. Amorphous material showing staining for transthyretin (E) but not with Congo red (F) is present in the subperineurial space (arrowheads). Bar = 40 μm.

dorsal root ganglion neurons were assessed using the image analyzer (Luzex FS). One hundred serial 10-μm-thick transverse sections at the middle portion of ganglia were prepared. Every tenth section was stained with the Klüver–Barrera method. Neurons showing obvious nucleoli in the sections were counted and measured to avoid split cell error. Number of neurons and area of ganglia on each section were assessed to calculate the density (neurons/mm^2). Values of neuronal cell density were expressed as means ± SD for these sections. For neuronal cell diameters, all neurons counted on 10 sections were measured. Values of neuronal cell diameter were expressed as means ± SD for these neurons. Control values for numbers and diameters of sympathetic and dorsal root ganglion neurons were obtained from four autopsy cases involving death from nonneurologic diseases.

Amounts of interstitial amyloid deposited in the parenchyma of various organs also were assessed using the Luzex FS analyzer. The proportion of area occupied by amyloid in each organ was determined as the extent of areas showing Congo red staining with emerald-green birefringence in polarized light and expressed as a percentage of the total transverse area. The proportion was assessed as the mean value for randomly selected areas covering at least 1 cm^2 of >10 sections. For nerve specimens, the proportion of area showing amyloid deposition to total endoneurial area was calculated. For the gastrointestinal tract, the proportion of area with amyloid deposition was assessed in the lamina muscularis mucosa.

Immunohistochemical assessment was performed with a peroxidase–antiperoxidase method using anti-human transthyretin antibody (Santa Cruz, CA) in consecutive deparaffinized sections.

Quantitative data, presented as means ± SD, were compared with control values. Statistical analyses were performed using the χ^2 test or the Mann–Whitney U test as appropriate. Values of p of <0.05 were considered to indicate significance.

Results. *Pathologic findings in sural nerve specimens.* In the early-onset cases, the density of large myelinated fibers was 914 ± 1,018 fibers/mm^2 (26% of age-matched normal control values) and that of small myelinated fibers was 451 ± 608 fibers/mm^2 (9% of age-matched normal control values), shown in table 2. Small myelinated fibers showed greater depletion than large myelinated fibers when myelinated fibers were not severely depleted overall (Cases 7 to 11). In late-onset cases, fiber size distribution

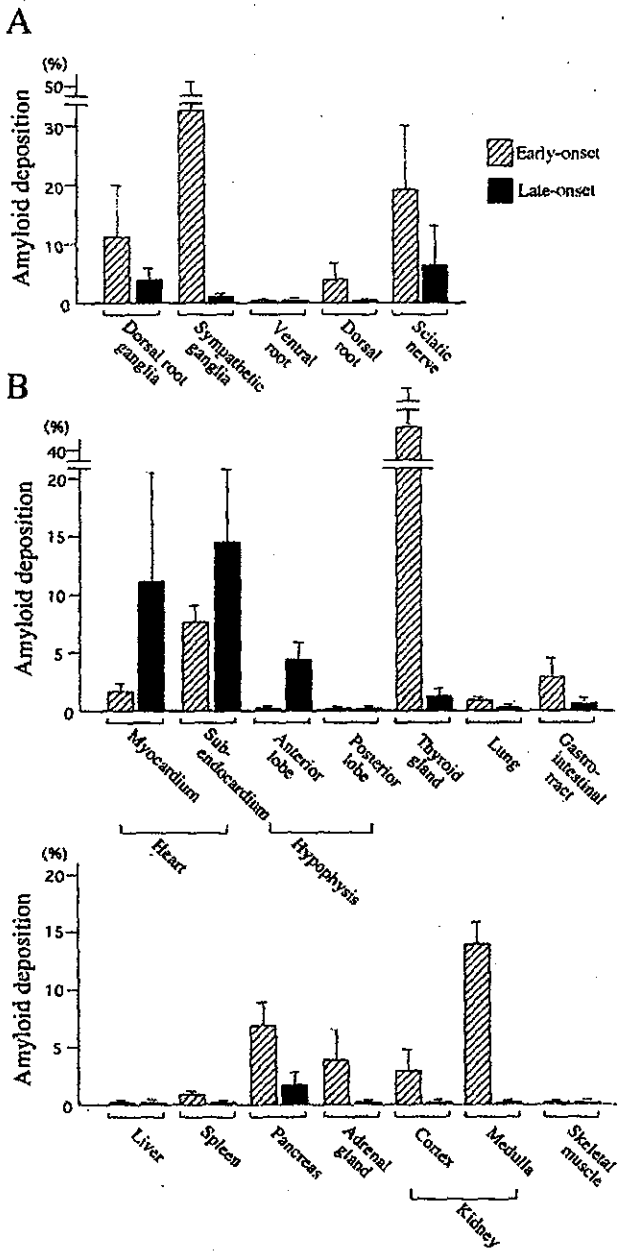

Figure 2. Amounts of interstitial amyloid deposited in the parenchyma of nervous system (A) and visceral organs (B). Hatched columns indicate mean values of early-onset cases (Cases 1 to 3), whereas filled columns indicate those of late-onset cases (Cases 12 to 14). Whiskers represent SDs. (A) Amyloid deposits in the nervous system are conspicuous in early-onset cases; these are less severe in late-onset cases. Amyloid deposition is more severe in sympathetic than dorsal root ganglia in early-onset cases, whereas the reverse pattern is seen in late-onset cases. (B) In early-onset cases, amyloid deposition is more prominent in the thyroid gland, gastrointestinal tract, pancreas, adrenal gland, and kidney than in late-onset cases. Amyloid deposition in early-onset cases is especially prominent in the thyroid gland and kidney, where deposition is scarce in late-onset cases. On the other hand, in late-onset cases, deposition is greater in the heart and anterior lobe of the hypophysis than in early-onset cases. Amyloid is scarce or absent in both groups in the posterior lobe of the pituitary gland, liver, and skeletal muscle.

of myelinated fibers, as indicated by the ratio of small to large myelinated fibers, was variable. Six cases (12, 14, 16 to 18, and 22) showed relative preservation of small myelinated fibers, whereas five cases (13, 15, 19 to 21) showed predominantly small-fiber loss as in early-onset cases. On average, density of large myelinated fibers was 333 ± 386 fibers/mm^2 (12% of age-matched normal control values) and that of small myelinated fibers was 789 ± 776 fibers/mm^2 (16% of age-matched normal control values). Axonal sprouting was scarce or absent in the early-onset group (5 ± 7/mm^2) but was relatively conspicuous in the late-onset group (92 ± 88/mm^2). Unmyelinated fibers were depleted more severely in the early- than the late-onset group (993 ± 1,305 vs 7,308 ± 5,417 fibers/mm^2; $p = 0.008$).

Amyloid deposition was scarce or absent in most cases in both groups, but relatively conspicuous deposition was observed in two of the early-onset cases (4 and 10). In both groups, amyloid was found in the endoneurium, both with and without relationship to small vessels.

Postmortem findings in the nervous system. Central nervous parenchyma was essentially intact in both groups, except that a small-cell carcinoma of the lung had metastasized to the cerebellum in Case 12, as previously described.[9,18] In the spinal cord, motor neurons as well as neurons in the Clarke columns were well preserved, and minimal to moderate myelinated fiber loss was observed in the posterior columns in both groups. Central chromatolysis was observed in spinal motor neurons in both groups. Amyloid deposits were not found in spinal cord parenchyma in any case.

In the dorsal root ganglia, amyloid deposits and neuronal cell loss were conspicuous in early-onset cases; these were less severe in late-onset cases (figures 1, A and B, and 2A). The mean diameter of remaining dorsal root ganglion neurons was larger in early-onset cases as compared with normal controls, suggesting predominant loss of small neurons (table 3). Mean neuronal cell diameters in late-onset cases were not notably different from those in normal controls, suggesting loss of neurons of all sizes. In the sympathetic ganglia, amyloid deposition and neuronal cell loss were very prominent in early-onset cases but less so in late-onset cases (see figures 1, C and D, and 2A). Size-selective neuronal cell loss was likely to be observed as in dorsal root ganglia (see table 3). Amyloid deposition and neuronal cell loss were more severe in sympathetic than dorsal root ganglia in early-onset cases, whereas the reverse pattern was seen in late-onset cases (see figure 2A and table 3). In the ventral spinal root, amyloid deposition was not apparent or only minimally present in both groups; likewise, myelinated fiber loss also was mild or not apparent in both groups. In the dorsal spinal root, amyloid deposition and myelinated fiber loss were moderately conspicuous in all early-onset cases but absent or minimal in late-onset cases. In sciatic and tibial nerves, amyloid deposition was more prominent in early-onset cases than the late-onset case (figure 3A). However, the late-onset case showed considerable myelinated fiber loss despite relative paucity of amyloid deposition (see figure 3B). In the median nerve, amyloid deposition also was more severe in early-onset cases than in the late-onset case, whereas myelinated fiber loss was more severe in the late-onset case than in early-onset cases. Amorphous material showing staining for transthyretin but not with Congo red was

Table 3 Neuronal cell loss and diameter in sympathetic and sensory ganglia

Case no.	Dorsal root ganglia		Sympathetic ganglia	
	Neuronal cell density, no./mm^2	Diameter of neurons in dorsal root ganglia, μm	Neuronal cell density, no./mm^2	Diameter of neurons in sympathetic ganglia, μm
Early-onset group				
1	4.0 ± 0.9	54.3 ± 8.6	4.2 ± 2.2	24.3 ± 3.8
2	1.9 ± 1.2	53.7 ± 8.8	4.0 ± 1.6	23.7 ± 4.2
3	2.6 ± 1.0	56.0 ± 9.0	1.6 ± 1.4	24.5 ± 3.3
Late-onset group				
12	7.5 ± 1.6	46.2 ± 11.4	46.2 ± 7.4	22.9 ± 4.6
13	4.8 ± 1.2	45.4 ± 9.1	44.8 ± 6.2	19.8 ± 4.6
14	5.8 ± 1.3	49.9 ± 11.4	ND	ND
Controls, n = 4	10.2 ± 3.2	48.3 ± 16.3	60.4 ± 6.6	20.0 ± 4.2

Values of neuronal cell density were expressed as means ± SD for densities on 10 sections as described in Patients and Methods. Values of neuronal cell diameter were expressed as means ± SD for all neurons counted on 10 sections. Control values were obtained from four autopsied cases.

ND = not determined.

abundant in the subperineurial space of the nerve trunk in the late-onset case (see figure 1, E and F), being less plentiful in early-onset cases.

Pathologic findings in visceral organs. In early-onset cases, amyloid deposition was more prominent in the thyroid gland, gastrointestinal tract, pancreas, adrenal gland, and kidney than in late-onset cases (figures 2B and 4). Amyloid deposition in early-onset cases was especially prominent in the thyroid gland and kidney, where deposition was scarce in late-onset cases. On the other hand, in late-onset cases, deposition was greater in the heart and the anterior pituitary lobe than in early-onset cases. Amyloid was scarce or absent in both groups in the posterior lobe of the pituitary gland, liver, and skeletal muscle. The heart weighed 420, 440, and 450 g in early-onset cases, whereas in late-onset patients dying of heart failure, it was 690 and 700 g. In a late-onset patient who died of lung cancer and had relatively short clinical duration of amyloid neuropathy, the heart weight was 380 g. In early-onset cases, cardiac amyloid deposition was prominent in the atrium and the subendocardial region. In the myocardium, amyloid was observed mainly in relation to walls of vessels, particularly arterioles. In the subendocardial layer, myocardial cells showed atrophy, degeneration, and eventual cell loss, producing a histologic picture of amyloid rings (see figure 4A). Among late-onset cases, amyloid was prominent throughout myocardium in two cases (13 and 14), whereas amyloid rings or atrophy of the myocardium was not apparent in any case (see figure 4B). The anterior lobe of the hypophysis showed scarce or no amyloid deposition in early-onset cases, but marked parenchymal deposition was observed in late-onset cases (see figure 4, C and D).

Discussion. In this study, we compared pathologic features of early-onset FAP TTR Met30 cases from endemic foci with those of late-onset cases from nonendemic areas. In anecdotal report of pathologic findings in FAP TTR Met30 patients presenting beyond age 50,[25] the distribution of amyloid deposition differed slightly from findings in the current study. Differences may be attributable to inclusion of late-onset cases from endemic foci in that report; these patients show clinical features similar to early-onset cases in endemic foci.[11] The current study demonstrated that pathologic features of the two groups differed, as has been shown for clinical features.[9-11]

The characteristic finding in early-onset cases was predominant loss of small fibers, including unmyelinated fibers; this agrees with previous reports.[26,27] On the other hand, fiber loss patterns in our late-onset cases were variable; half of the cases showed predominantly small-fiber loss as in early-onset cases, whereas others showed relative preservation of small myelinated fibers. As a whole, the total number of myelinated fibers was more severely reduced in late- than early-onset cases. This difference correlated well with the prominent sensory dissociation noted in early-onset cases in contrast to impairment of all modalities in late-onset cases.[3,9,11] The finding that amyloid deposition and neuronal cell loss were more severe in sympathetic than sensory ganglia in early-onset cases—with the reverse pattern seen in late-onset cases—also correlated with the severity of autonomic symptoms.[3,7-9,11] Furthermore, preferential loss of small neurons in the sensory ganglia in early-onset cases and loss of neurons of all sizes in late-onset cases, as suggested by the mean diameter of remaining neurons, corresponded to clinical differences in sensory involvement. Amyloid deposition and atrophy of myocardial cells in the atrium and subendocardial layer of the myocardium, where the cardiac conduction system is located, explains a more frequent occurrence of cardiac conduction abnormalities and need for pacemaker implantation in early- than late-onset cases.[3,11] On the other hand, diffuse deposition of amyloid with ventricular wall thickening agrees well with frequent observations of cardiac hypertrophy and occur-

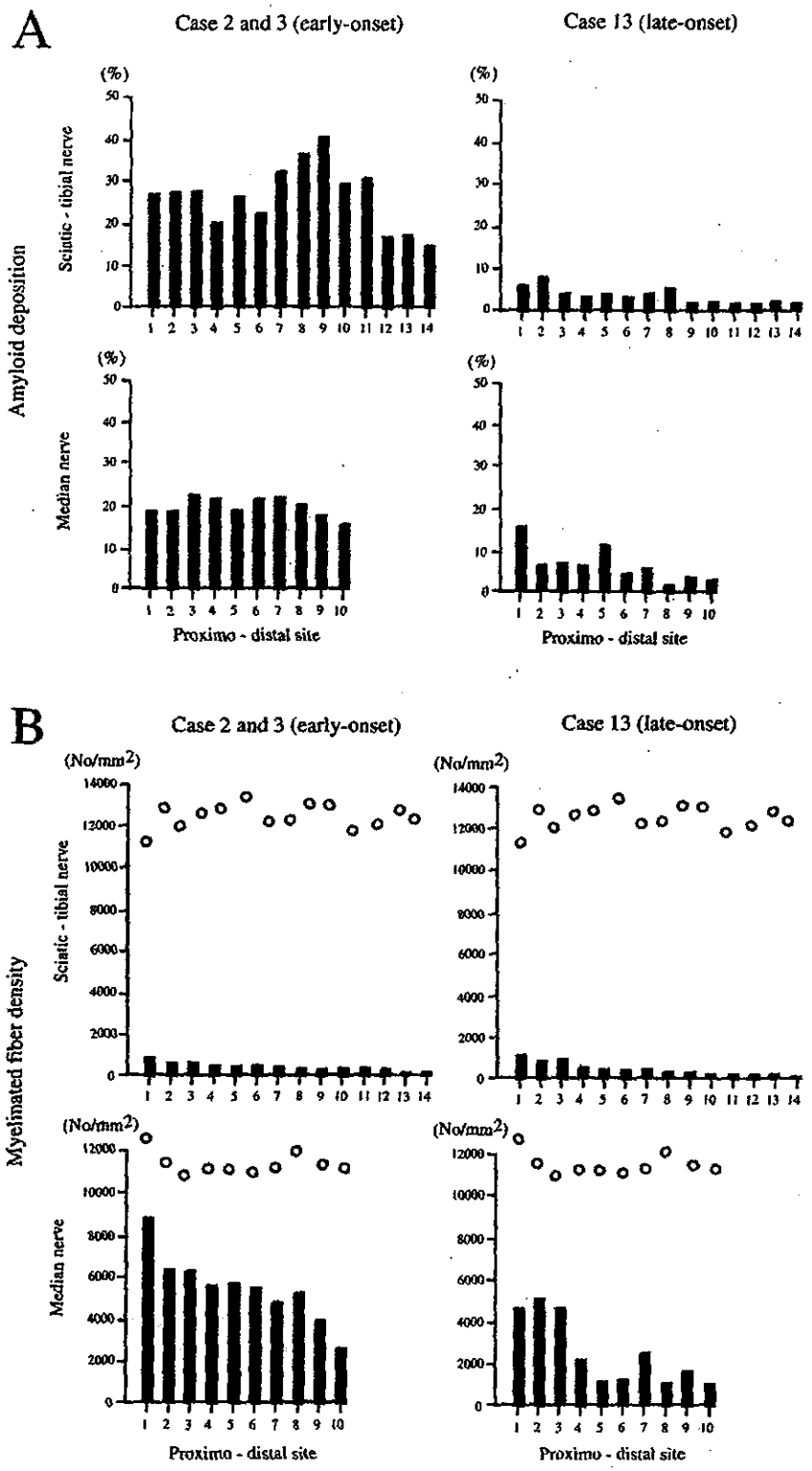

Figure 3. Proportion of amyloid deposition in the endoneurium (A) and density of myelinated fibers (B) in consecutive portions of the sciatic/tibial and median nerves from early-onset cases (Cases 2 and 3) and late-onset case (Case 13). Values for early-onset cases are represented as the means of Cases 2 and 3. Open circles represent normal control values obtained from a subject with nonneurologic disease. In sciatic and tibial nerves, amyloid deposition is more prominent in early-onset cases than in the late-onset case. However, the late-onset case showed considerable myelinated fiber loss despite relative paucity of amyloid deposition. In the median nerve, amyloid deposition also is more severe in early-onset cases than in the late-onset case, whereas myelinated fiber loss is more severe in the late-onset case than in early-onset cases.

rence of heart failure in late-onset cases.[9] Thus, differences in clinical features reported between early- and late-onset FAP TTR Met30 corresponded well to pathologic differences.

A question remains as to why the severity and distribution pattern of amyloid deposition differ between early- and late-onset cases. A longer interval from onset of neuropathic symptoms to autopsy in the early-onset group may explain some of the pathologic differences. The peripheral nervous system, thyroid gland, gastrointestinal tract, pancreas, adrenal gland, and kidney showed more severe amyloid deposition in the early-onset group, consistent with a longer duration of illness. However, the heart and hypophysis showed more prominent deposition in the late-onset group, which had a shorter clinical disease duration. The diffuse amyloid deposition observed in the ventricular myocardium in late-onset cases is

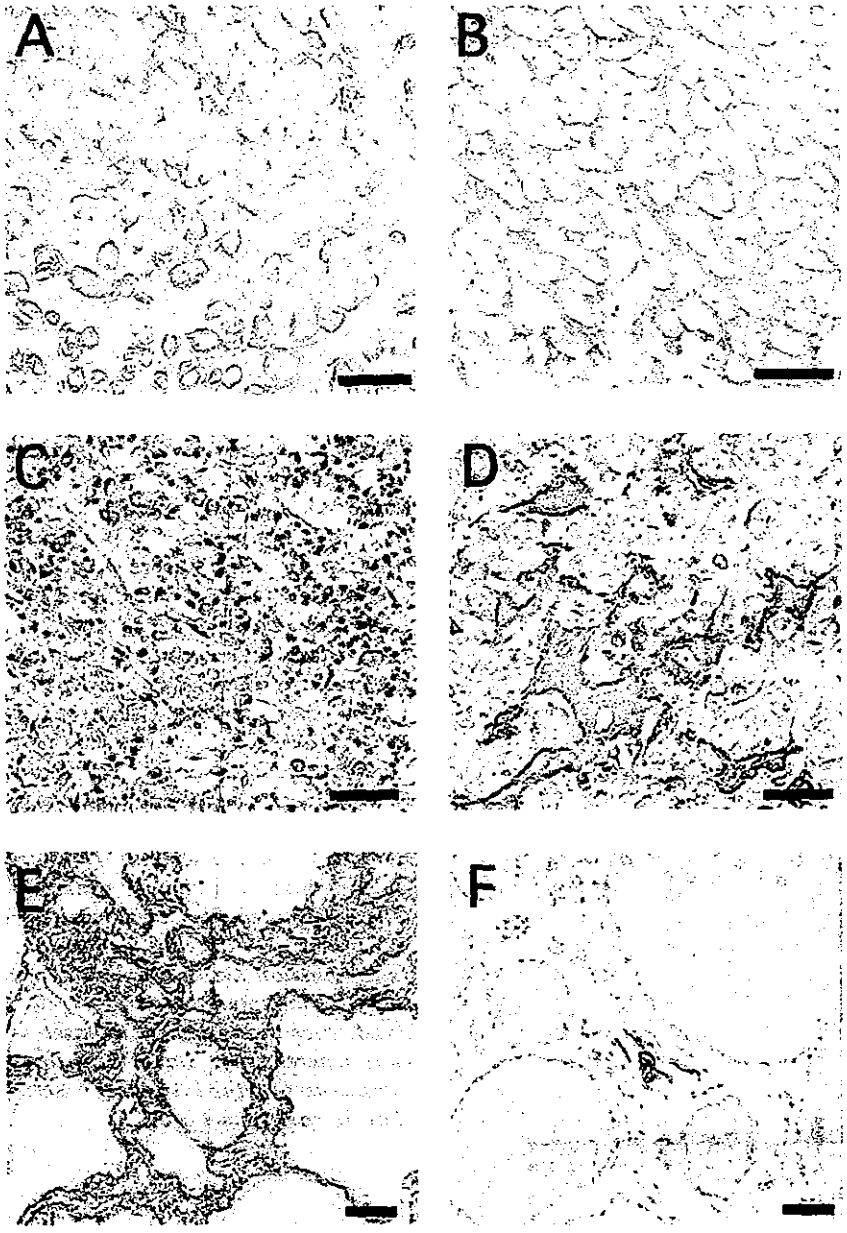

Figure 4. Representative pathologic findings in the visceral organs from early-onset cases (left) and late-onset cases (right). Amyloid deposits are identified by anti-human transthyretin antibody. (A, B) The heart. In the subendocardial layer of an early-onset case (A), myocardial cells show atrophy and amyloid rings are present. In late-onset cases, amyloid is prominent throughout myocardium (B). Amyloid rings or atrophy of the myocardium is not apparent as in (A). (C, D) Anterior lobe of the pituitary gland. Amyloid deposition is scarce in early-onset cases (C), whereas it is conspicuous in late-onset cases (D). (E, F) The thyroid gland. Amyloid deposition was especially prominent in early-onset cases (E), but it was scarce in late-onset cases (F). Bar = 40 μm.

similar to that of senile cardiac amyloidosis with deposition of normal transthyretin protein.[28] Age-related accumulation of amyloid in the interstitium of the anterior lobe of the pituitary gland also has been reported.[29-31] These observations suggest that age-dependent changes in the microenvironment of interstitial tissues in various organs determine the severity and distribution pattern of amyloid deposition in each group. For example, properties of extracellular matrix components including proteoglycans and glycosaminoglycans, which may become components of amyloid,[32] show organ-specific changes with age.[33,34] Interestingly, the posterior lobe of the hypophysis, the liver, and skeletal muscle did not show detectable amyloid deposition in cases with either age at onset. Mechanisms of underlying organ-specific, age-related amyloid deposition still need to be elucidated, but age at onset itself may influence some of the organ-specific amyloid deposition patterns.

Another question remaining is why size dependence of axonal and neuronal cell loss differed between early- and late-onset cases. Even after taking axonal sprouting into account, small myelinated and unmyelinated fibers seemed relatively well preserved in many late-onset cases. Although the pathogenesis of peripheral neuropathy in amyloidosis has not yet been clarified, possibilities might include ischemia from obliteration or dysfunction of small vessels supplying nerves,[35,36] nerve fiber compression or infiltration by amyloid deposits,[26,37] or toxic effects of amyloid precursors.[38-40] Experiments in animals as well as human studies suggest that the nonfibrillar form of transthyretin is present in tissues and exerts cytotoxicity, including oxidative stress,[40] before the congophilic fibrillar form of amyloid can be seen.[38,41]

The concept that a nonfibrillar precursor of amyloid can exert toxic effects can be extended to other pathologic conditions where amyloid is considered pathogenetically important, including Alzheimer disease.[42-45] In our study, amyloid was not deposited in late-onset cases until patients had become elderly, considering that amyloid deposition was scarce or absent in sural nerve biopsy specimens. Accumulation of amyloid may progress rapidly once initiated. Abundant nerve fiber regeneration despite scarce amyloid deposition was observed in most sural nerve biopsy specimens from our late-onset cases, indicating that axons had been degenerating long before amyloid deposition occurred in these cases. At autopsy, less amyloid deposition but severe myelinated fiber loss in nerve trunks from a late-onset case in comparison with early-onset cases support this view. Furthermore, amorphous material staining with anti-transthyretin antibody but not with Congo red, indicating presence of the nonfibrillar amyloid precursor, was more abundant in the late-onset case. Taken together, these observations support cytotoxicity from nonfibrillar transthyretin affecting all sizes of axons and neurons prior to deposition of congophilic amyloid in late-onset cases. In early-onset cases, amyloid deposition was likely to have been severe even in early stages, judging from amounts of amyloid observed. Nerve fiber compression by amyloid deposits could cause predominantly small-fiber loss, as previously suggested.[26] Differential duration of exposure to a toxic amyloid precursor may result in pathologically different modes of axonal and neuronal cell loss.

References

1. Andrade C. A peculiar form of peripheral neuropathy. Familial atypical generalized amyloidosis with special involvement of the peripheral nerves. Brain 1952;75:408–427.
2. Benson MD, Cohen AS. Generalized amyloid in a family of Swedish origin. A study of 426 family members in seven generations of a new kinship with neuropathy, nephropathy, and central nervous system involvement. Ann Intern Med 1977;86:419–424.
3. Ikeda S, Hanyu N, Hongo M, et al. Hereditary generalized amyloidosis with polyneuropathy: clinicopathological study of 65 Japanese patients. Brain 1987;110:315–337.
4. Nakazato M, Shiomi K, Miyazato M, Matsukura S. Type 1 familial amyloidotic polyneuropathy in Japan. Intern Med 1992;31:1335–1338.
5. Sousa A, Coelho T, Barros J, Sequeiros J. Genetic epidemiology of familial amyloidotic polyneuropathy (FAP)-type I in Povoa do Varzim and Vila do Conde (north of Portugal). Am J Med Genet 1995;60:515–521.
6. Reilly MM, Adams D, Booth DR, et al. Transthyretin gene analysis in European patients with suspected familial amyloid polyneuropathy. Brain 1995;118:849–856.
7. Ando Y, Araki S, Shimoda O, Kano T. Role of autonomic nerve functions in patients with familial amyloidotic polyneuropathy as analyzed by laser Doppler flowmetry, capsule hydrograph, and cardiographic R-R interval. Muscle Nerve 1992;15:507–512.
8. Ando Y, Suhr OB. Autonomic dysfunction in familial amyloid polyneuropathy (FAP). Amyloid Int J Exp Clin Invest 1998;5:288–300.
9. Misu K, Hattori N, Nagamatsu M, et al. Late-onset familial amyloid polyneuropathy type I (transthyretin Met 30-associated familial amyloid polyneuropathy) unrelated to endemic focus in Japan; clinicopathological and genetic features. Brain 1999;122:1951–1962.
10. Misu K, Hattori N, Ando Y, Ikeda S, Sobue G. Anticipation in early- but not late-onset familial amyloid polyneuropathy (TTR met 30) in Japan. Neurology 2000;55:451–452.
11. Koike H, Misu K, Ikeda S, et al. Type I (transthyretin Met30) familial amyloid polyneuropathy in Japan: early- versus late-onset form. Arch Neurol 2002;59:1771–1776.
12. Sobue G, Koike H, Misu K, et al. Clinicopathologic features of early- and late-onset FAP type I (FAP ATTR Val30Met) in Japan. Amyloid J Protein Folding Disord 2003;1(suppl):32–38.
13. Coelho T, Sousa A, Lourenco E, Ramalheira J. A study of 159 Portuguese patients with familial amyloidotic polyneuropathy (FAP) whose parents were both unaffected. J Med Genet 1994;31:293–299.
14. Saravia MJ, Costa PP, Goodman DS. Genetic expression of a transthyretin mutation in typical and late-onset Portuguese families with familial amyloidotic polyneuropathy. Neurology 1986;36:1413–1417.
15. Sasaki Y, Yoshioka K, Tanahashi H, Furuya H, Sasaki H. Human transthyretin (prealbumin) gene and molecular genetics of familial amyloidotic polyneuropathy. Mol Biol Med 1989;6:161–168.
16. Sobue G, Yasuda T, Mitsuma T, Loss AH, Pleasure D. Expression of nerve growth factor receptor in human peripheral neuropathies. Ann Neurol 1988;24:64–72.
17. Sobue G, Hashizume Y, Mukai E, et al. X-linked recessive bulbospinal neuronopathy, a clinicopathological study. Brain 1989;112:209–232.
18. Sobue G, Nakao N, Murakami K, et al. Type I familial amyloid polyneuropathy. A pathological study of the peripheral nervous system. Brain 1990;113:903–919.
19. Hattori N, Ichimura M, Nagamatsu M, et al. Clinicopathological features of Churg–Strauss syndrome-associated neuropathy. Brain 1999; 122:427–439.
20. Koike H, Mori K, Misu K, et al. Painful alcoholic polyneuropathy with predominant small-fiber loss and normal thiamine status. Neurology 2001;56:1727–1732.
21. Koike H, Iijima M, Sugiura M, et al. Alcoholic neuropathy is clinicopathologically distinct from thiamine-deficiency neuropathy. Ann Neurol 2003;54:19–29.
22. Hattori N, Yamamoto M, Yoshihara T, et al. Demyelinating and axonal features of Charcot–Marie–Tooth disease with mutations of myelin-related proteins (PMP22, MPZ and Cx32): a clinicopathological study of 205 Japanese patients. Brain 2003;126:134–151.
23. Dyck PJ, Giannini C, Lais A. Pathologic alterations of nerves. In: Dyck PJ, Thomas PK, Griffin JW, Low PA, Poduslo JF, eds. Peripheral neuropathy. 3rd ed. Philadelphia: Saunders, 1993:514–595.
24. Nagamatsu M, Terao S, Misu K, et al. Axonal and perikaryal involvement in chronic inflammatory demyelinating polyneuropathy. J Neurol Neurosurg Psychiatry 1999;66:727–733.
25. Takahashi K, Sakashita N, Ando Y, Suga M, Ando M. Late onset type I familial amyloidotic polyneuropathy: presentation of three autopsy cases in comparison with 19 autopsy cases of the ordinary type. Pathol Int 1997;47:353–359.
26. Said G, Ropert A, Faux N. Length-dependent degeneration of fibers in Portuguese amyloid polyneuropathy: a clinicopathologic study. Neurology 1984;34:1025–1032.
27. Takahashi K, Yi S, Kimura Y, Araki S. Familial amyloidotic polyneuropathy type 1 in Kumamoto, Japan: a clinicopathologic, histochemical, immunohistochemical, and ultrastructural study. Hum Pathol 1991;22: 519–527.
28. Olson LJ, Gertz MA, Edwards WD, et al. Senile cardiac amyloidosis with myocardial dysfunction. Diagnosis by endomyocardial biopsy and immunohistochemistry. N Engl J Med 1987;317:738–742.
29. Tashima T, Kitamoto T, Tateishi J, Ogomori K, Nakagaki H. Incidence and characterization of age related amyloid deposits in the human anterior pituitary gland. Virchows Arch A Pathol Anat Histopathol 1988;412:323–327.
30. Röcken C, Eick B, Saeger W. Senile amyloidosis of the pituitary and adrenal glands. morphological and statistical investigations. Virchows Arch 1996;429:293–299.
31. Westermark P, Eriksson L, Engstrom U, Enestrom S, Sletten K. Prolactin-derived amyloid in the aging pituitary gland. Am J Pathol 1997;150:67–73.
32. Magnus JH, Stenstad T. Proteoglycans and the extracellular matrix in amyloidosis. Amyloid J Exp Clin Invest 1997;4:121–134.
33. Nakayama Y, Narita T, Mori A, Uesaka S, Miyazaki K, Ito H. The effects of age and sex on chondroitin sulfates in normal synovial fluid. Arthritis Rheum 2002;46:2105–2108.
34. Carrino DA, Onnerfjord P, Sandy JD, et al. Age-related changes in the proteoglycans of human skin. Specific cleavage of decorin to yield a major catabolic fragment in adult skin. J Biol Chem 2003;278:17566–17572.
35. Hanyu N, Ikeda S, Nakadai A, Yanagisawa N, Powell HC. Peripheral nerve pathological findings in familial amyloid polyneuropathy: a correlative study of proximal sciatic nerve and sural nerve lesions. Ann Neurol 1989;25:340–350.
36. Berghoff M, Kathpal M, Khan F, Skinner M, Falk R, Freeman R. Endothelial dysfunction precedes C-fiber abnormalities in primary (AL) amyloidosis. Ann Neurol 2003;53:725–730.
37. Dyck PJ, Lambert EH. Dissociated sensation in amyloidosis. Compound action potential, quantitative histologic and teased-fiber, and electron microscopic studies of sural nerve biopsies. Arch Neurol 1969;20:490–507.
38. Sousa MM, Cardoso I, Fernandes R, Guimaraes A, Saraiva MJ. Deposition of transthyretin in early stages of familial amyloidotic polyneuropathy: evidence for toxicity of nonfibrillar aggregates. Am J Pathol 2001; 159:1993–2000.
39. Andersson K, Olofsson A, Nielsen EH, Svehag SE, Lundgren E. Only amyloidogenic intermediates of transthyretin induce apoptosis. Biochem Biophys Res Commun 2002;294:309–314.

40. Fiszman ML, Di Egidio M, Ricart KC, et al. Evidence of oxidative stress in familial amyloidotic polyneuropathy type 1. Arch Neurol 2003;60: 593–597.
41. Sousa MM, Fernandes R, Palha JA, Taboada A, Vieira P, Saraiva MJ. Evidence for cytotoxic aggregates in transgenic mice for human transthyretin Leu55Pro. Am J Pathol 2002;161:1935–1948.
42. LaFerla FM, Tinkle BT, Bieberich CJ, Haudenschild CC, Jay G. The Alzheimer's Abeta peptide induces neurodegeneration and apoptotic cell death in transgenic mice. Nat Genet 1995;9:21–30.
43. Hartley DM, Walsh DM, Ye CP, et al. Protofibrillar intermediates of amyloid beta-protein induce acute electrophysiological changes and progressive neurotoxicity in cortical neurons. J Neurosci 1999;19:8876–8884.
44. McLean CA, Cherny RA, Fraser FW, et al. Soluble pool of Abeta amyloid as a determinant of severity of neurodegeneration in Alzheimer's disease. Ann Neurol 1999;46:860–866.
45. Kayed R, Head E, Thompson JL, et al. Common structure of soluble amyloid oligomers implies common mechanism of pathogenesis. Science 2003;300:486–489.

THE JOURNAL OF BIOLOGICAL CHEMISTRY
Vol. 279, No. 49, Issue of December 3, pp. 51376–51385, 2004
Printed in U.S.A.

Physical and Functional Interaction between Dorfin and Valosin-containing Protein That Are Colocalized in Ubiquitylated Inclusions in Neurodegenerative Disorders*

Received for publication, June 15, 2004, and in revised form, August 31, 2004
Published, JBC Papers in Press, September 29, 2004, DOI 10.1074/jbc.M406683200

Shinsuke Ishigaki‡§¶, Nozomi Hishikawa‡, Jun-ichi Niwa‡, Shun-ichiro Iemura‖, Tohru Natsume‖, Seiji Hori, Akira Kakizuka**‡‡, Keiji Tanaka§, and Gen Sobue‡§§**

*From the ‡Department of Neurology, Nagoya University Graduate School of Medicine, Nagoya 466-8500, Japan, the §Department of Molecular Oncology, Tokyo Metropolitan Institute of Medical Science, Tokyo 113-8613, Japan, the ‖National Institute of Advanced Science and Technology, Biological Information Research Center, Tokyo 135-0064, Japan, the **Laboratory of Functional Biology, Kyoto University Graduate School of Biostudies, Kyoto 606-8502, Japan, and ‡‡CREST, Japan Science and Technology Agency, Kawaguchi 332-0012, Japan*

Dorfin, a RING-IBR type ubiquitin ligase (E3), can ubiquitylate mutant superoxide dismutase 1, the causative gene of familial amyotrophic lateral sclerosis (ALS). Dorfin is located in ubiquitylated inclusions (UBIs) in various neurodegenerative disorders, such as ALS and Parkinson's disease (PD). Here we report that Valosin-containing protein (VCP) directly binds to Dorfin and that VCP ATPase activity profoundly contributes to the E3 activity of Dorfin. High through-put analysis using mass spectrometry identified VCP as a candidate of Dorfin-associated protein. Glycerol gradient centrifugation analysis showed that endogenous Dorfin consisted of a 400–600-kDa complex and was co-immunoprecipitated with endogenous VCP. *In vitro* experiments showed that Dorfin interacted directly with VCP through its C-terminal region. These two proteins were colocalized in aggresomes in HEK293 cells and UBIs in the affected neurons of ALS and PD. VCP^{E524A}, a dominant negative form of VCP, reduced the E3 activity of Dorfin against mutant superoxide dismutase 1, whereas it had no effect on the autoubiquitylation of Parkin. Our results indicate that VCPs functionally regulate Dorfin through direct interaction and that their functional interplay may be related to the process of UBI formation in neurodegenerative disorders, such as ALS or PD.

Amyotrophic lateral sclerosis (ALS)[1] is one of the most common neurodegenerative disorders, characterized by selective motor neuron degeneration in the spinal cord, brain stem, and cortex. Two genes, CuZn-superoxide dismutase (SOD1) and amyotrophic lateral sclerosis 2 have been identified as responsible genes for familial forms of ALS. Using mutant SOD1 transgenic mice, the pathogenesis of ALS has been partially uncovered. The proposed mechanisms of the motor neuron degeneration in ALS include oxidative toxicity, glutamate receptor abnormality, ubiquitin proteasome dysfunction, inflammatory and cytokine activation, dysfunction of neurotrophic factors, damage to mitochondria, cytoskeletal abnormalities, and activation of the apoptosis pathway (1, 2).

In a previous study (3), we identified several ALS-associated genes using molecular indexing. Dorfin was identified as one of the up-regulated genes in ALS, which contains a RING-IBR (in between ring finger) domain at its N terminus and mediated ubiquitin ligase (E3) activity (3, 4). Dorfin colocalized with Vimentin at the centrosome after treatment with a proteasome inhibitor in cultured cells (4). Dorfin physically bound and ubiquitylated various SOD1 mutants derived from familial ALS patients and enhanced their degradation, but it had no effect on the stability of wild-type SOD1 (5). Overexpression of Dorfin protected neural cells against the toxic effects of mutant SOD1 and reduced SOD1 inclusions (5).

Recent findings indicate that the ubiquitin-proteasome system is widely involved in the pathogenesis of Parkinson's disease (PD), Alzheimer's disease, polyglutamine disease, and Prion diseases as well as ALS (6). From this point of view, we previously analyzed the pathological features of Dorfin in various neurodegenerative diseases and found that Dorfin was predominantly localized not only in Lewy body (LB)-like inclusions in ALS but also in LBs in PD, dementia with Lewy bodies, and glial cell inclusions in multiple system atrophy (7). These characteristic intracellular inclusions composed of aggregated, ubiquitylated proteins surrounded by disorganized filaments are the histopathological hallmark of aging-related neurodegenerative diseases (8).

A structure called aggresome by Johnston *et al.* (9) is formed when the cell capacity to degrade misfolded proteins is exceeded. The aggresome has been defined as a pericentriolar, membrane-free, cytoplasmic inclusion containing misfolded ubiquitylated protein ensheathed in a cage of intermediate filaments, such as Vimentin (9). The formation of the aggresome mimics that of ubiquitylated inclusions (UBIs) in the affected neurons of various neurodegenerative diseases (10). Combined with the fact that Dorfin was localized in aggresomes in cultured cells and UBIs in ALS and other neurode-

* This work was supported by a grant for a Center of Excellence from the Ministry of Education, Culture, Sports, Science, and Technology of Japan. The costs of publication of this article were defrayed in part by the payment of page charges. This article must therefore be hereby marked "*advertisement*" in accordance with 18 U.S.C. Section 1734 solely to indicate this fact.

¶ Research resident of the Japan Foundation for Aging and Health, Psychiatric and Neurological Diseases, and Mental Health.

§§ To whom correspondence should be addressed: Dept. of Neurology, Nagoya University Graduate School of Medicine, Nagoya 466-8500, Japan. Tel.: 81-52-744-2385; Fax: 81-52-744-2384; E-mail: sobueg@med.nagoya-u.ac.jp.

[1] The abbreviations used are: ALS, amyotrophic lateral sclerosis; E3, ubiquitin ligase; ERAD, endoplasmic reticulum-associated degradation; LB, Lewy body; MS, mass spectrometry; LC-MS/MS, liquid chromatography coupled to electrospray tandem mass spectrometry; PD, Parkinson's disease; SOD1, CuZn-superoxide dismutase; UBI, ubiquitylated inclusions; VCP, valosin-containing protein; FLAG-Parkin, pcDNA3.1/FLAG-Parkin; Ub, ubiquitin; MBP, maltose-binding protein; GST, glutathione *S*-transferase; PBS, phosphate-buffered saline; HA, hemagglutinin; WT, wild type.

generative diseases, these observations suggest that Dorfin may have a significant role in the quality control system in the cell. The present study was designed to obtain further clues for the pathophysiological roles of Dorfin. For this purpose, we screened Dorfin-associated proteins using high performance liquid chromatography coupled to electrospray tandem mass spectrometry (LC-MS/MS). The results showed that Valosin-containing protein (VCP), also called p97 or Cdc48 homologue, obtained from the screening, physically and functionally interacted with Dorfin. Furthermore, both Dorfin and VCP proteins colocalized in aggresomes of the cultured cells and in UBIs in various neurodegenerative diseases.

MATERIALS AND METHODS

Plasmids and Antibodies—pCMV2/FLAG-Dorfin vector (FLAG-Dorfin^{WT}) was prepared by PCR using the appropriate design of PCR primers with restriction sites (ClaI and KpnI). The PCR product was digested and inserted into the ClaI-KpnI site in pCMV2 vector (Sigma). pEGFP-Dorfin (GFP-Dorfin), pCMX-VCP^{Wt} (VCP^{Wt}), and pCMX-VCP^{K524A} (VCP^{K524A}) vectors were described previously (5, 11). pcDNA/HA-VCP^{Wt} (HA-VCP^{Wt}) and pcDNA/HA-VCP^{K524A} (HA-VCP^{K524A}) were subcloned from pCMX-VCP^{Wt} and pCMX-VCP^{K524A}, respectively, into pcDNA3.1 vectors (Invitrogen). The HA tag was introduced at the N terminus of VCP. pcDNA3.1/FLAG-Parkin (FLAG-Parkin) was generated by PCR using the appropriate design of PCR primers with restriction sites (EcoRI and NotI) from pcDNA3.1/Myc-Parkin (12). The FLAG tag was introduced at the N terminus of Parkin. To establish the RING mutant plasmid of Dorfin (FLAG-Dorfin$^{C132S/C135S}$), point mutations for Cys at positions 132 and 135 to Ser were generated by PCR-based site-directed mutagenesis using a QuikChange™ site-directed mutagenesis kit (Stratagene, La Jolla, CA). pcDNA3.1/HA-Ub (HA-Ub), pcDNA3.1/Myc-SOD1^{WT} (SOD1^{WT}-Myc), pcDNA3.1/Myc-SOD1^{G93A} (SOD1^{G93A}-Myc), and pcDNA3.1/Myc-SOD1^{G85R} (SOD1^{G85R}-Myc) were described previously (13, 14). Polyclonal anti-Dorfin (Dorfin-30 and Dorfin-41) and monoclonal anti-VCP antibodies were used as in previous reports (5, 15). The following antibodies were used in this study: monoclonal anti-FLAG antibody (M2; Sigma), monoclonal anti-Myc antibody (9E10; Santa Cruz Biotechnology, Santa Cruz, CA), monoclonal anti-HA antibody (12CA5; Roche Applied Science), polyclonal anti-maltose-binding protein (MBP) antibody (New England BioLabs, Beverly, MA), polyclonal anti-Parkin (Cell Signaling, Beverly, MA), and polyclonal anti-SOD1 (SOD-100; Stressgen, San Diego, CA).

Cell Culture and Transfection—All media and reagents for cell culture were purchased from Invitrogen. HEK293 cells were grown in Dulbecco's modified Eagle's medium containing 10% fetal calf serum, 5 units/ml penicillin, and 50 μg/ml streptomycin. HEK293 cells at subconfluence were transfected with the indicated plasmids using FuGENE6 reagent (Roche Applied Science). To inhibit cellular proteasome activity, cells were treated with 1 μM MG132 (benzyloxycarbonyl-Leu-Leu-Leu-al; Sigma) for 16 h after overnight post-transfection. Cells were analyzed at 24–48 h after transfection.

Protein Identification by LC-MS/MS Analysis—FLAG-Dorfin^{WT} was expressed in HEK293 cells (semiconfluent in a 10-cm dish) and then immunoprecipitated by anti-FLAG antibody. The immunoprecipitates were eluted with a FLAG peptide and then digested with Lys-C endopeptidase (*Achromobacter* protease I). The resulting peptides were analyzed using a nanoscale LC-MS/MS system as described previously (16). The peptide mixture was applied to a Mightysil-PR-18 (1-μm particle, Kanto Chemical Corp., Tokyo) column (45 × 0.150 mm ID) and separated using a 0–40% gradient of acetonitrile containing 0.1% formic acid over 30 min at a flow rate of 50 nl/min. Eluted peptides were sprayed directly into a quadrupole time-of-flight hybrid mass spectrometer (Q-Tof *Ultima*; Micromass, Manchester, UK). MS and MS/MS spectra were obtained in data-dependent mode. Up to four precursor ions above an intensity threshold of 10 cps were selected for MS/MS analysis from each survey scan. All MS/MS spectra were searched against protein sequences of Swiss Prot and RefSeq (NCBI) using batch processes of the Mascot software package (Matrix Science, London, UK). The criteria for match acceptance were the following: 1) when the match score was 10 over each threshold, identification was accepted without further consideration; 2) when the difference of score and threshold was lower than 10 or when proteins were identified based on a single matched MS/MS spectrum, we manually confirmed the raw data prior to acceptance; 3) peptides assigned by less than three y series ions and peptides with +4 charge state were all eliminated regardless of their scores.

Recombinant Proteins and Pull-down Assay—We used pMALp2 (New England BioLabs) and pMALp2T (Factor Xa cleavage site of pMALp2 was replaced with a thrombin recognition site) to express fusion proteins with MBP. To produce the full-length (residues 1–838) Dorfin (MBP-Dorfin^{full}), N-terminal (residues 1–367) Dorfin (MBP-Dorfin^{N}), and C-terminal (residues 368–838) Dorfin (MBP-Dorfin^{C}), the PCR fragments were amplified from pcDNA4/HisMax-Dorfin (4) by using the appropriate PCR primers with restriction sites (FbaI and HindIII) and then ligated into pMAL-p2 vectors. To produce the MBP-Parkin protein, full-length *PARKIN* cDNA was inserted into the EcoRI-NotI sites of pMALp2T. All of the MBP-tagged recombinant proteins were purified from *Escherichia coli* BL21-codon-plus. The detail of the purification method of MBP-tagged proteins was described previously (17). Recombinant GST fusion VCP^{WT} and VCP^{K524A} proteins were also generated from *E. coli* lysate and purified with glutathione-Sepharose. Recombinant His-VCP^{WT} and His-VCP^{K524A} proteins were purified from insect cells using baculovirus. The detail of purification of these recombinant VCP proteins was described previously (15). Binding experiments were performed with proteins carrying different tags. His- or GST-VCP were mixed with MBP fusion proteins: MBP-Dorfin^{full}, -Dorfin^{N}, -Dorfin^{C}, -Parkin, and -mock. His-VCP and GST-VCP proteins were precipitated by Ni^{2+}-nitrilotriacetic acid-agarose (Qiagen, Valencia, CA), and glutathione-Sepharose (Amersham Biosciences), respectively. Binding was performed with 1–3 μg of each protein in 300 μl of binding buffer (50 mM Tris-HCl, pH 7.5, 100 mM NaCl, 5 mM $MgCl_2$, 10% glycerol, 0.5 mg/ml bovine serum albumin, 1 mM dithiothreitol) for 1 h at 4 °C. Then 15 μl of beads were added and incubated for 30 min. The beads were washed by binding buffer three times and eluted with sample buffer and analyzed by SDS-PAGE followed by Western blotting using specific antibodies.

Glycerol Gradient Centrifugation—Cultured cells or mouse tissues were homogenized in 1 ml of PBS with protease inhibitor (Complete Mini; Roche Applied Science). Supernatants (1 mg of protein for cultured cells, 5 mg of protein for mouse tissues, and 0.1 mg of recombinant His-VCP protein) were used as the samples after 10,000 × *g* centrifugation for 20 min. The samples (1.0 ml) were loaded on top of a 34-ml linear gradient of glycerol (10–40%) prepared in 25 mM Tris-HCl buffer, pH 7.5, containing 1 mM dithiothreitol in 40 PA centrifuge tubes (Hitachi, Tokyo), and centrifuged at 4 °C and 80,000 × *g* for 22 h using a Himac CP100α centrifuge system (Hitachi). Thirty fractions were collected from the top of the tubes. Two hundred μl of each fraction was precipitated with acetone, and the remaining pellet was lysed with 50 μl of sample buffer and then used for SDS-PAGE followed by Western blotting.

Immunological Analysis—Cells (4 × 10^5 in a 6-cm dish) were lysed with 500 μl of lysis buffer (50 mM Tris-HCl, 150 mM NaCl, 1% Nonidet P-40, and 1 mM EDTA) with protease inhibitor mixture (Complete Mini) 24–48 h after transfection. The lysate was then centrifuged at 10,000 × *g* for 10 min at 4 °C to remove debris. A 10% volume of the supernatants was used as the "lysate" for SDS-PAGE. When immunoprecipitated, the supernatants were precleared with protein A-Sepharose (Amersham Biosciences), and specific antibodies, anti-FLAG (M2), anti-Myc (9E10), or anti-Dorfin (Dorfin-30) were then added and then incubated at 4 °C with rotation. Immune complexes were then incubated with protein A-Sepharose for 3 h, collected by centrifugation, and washed four times with the lysis buffer. For protein analysis, immune complexes were dissociated by heating in SDS-PAGE sample buffer and loaded onto SDS-PAGE. The samples were separated by SDS-PAGE (12% gel or 4–12% gradient gel) and transferred onto a polyvinylidene difluoride membrane. Finally, Western blotting was performed with specific antibodies.

Immunohistochemistry—HEK293 cells grown on glass coverslips were fixed in 4% paraformaldehyde in PBS for 15 min. Then the cells were blocked for 30 min with 5% (v/v) normal goat serum in PBS, incubated for 1 h at 37 °C with anti-HA antibody (12CA5), washed with PBS, and incubated for 30 min with Alexa 496-nm anti-mouse antibodies (Molecular Probes, Inc., Eugene, OR). The coverslips were washed and mounted on slides. Fluorescence images were obtained using a fluorescence microscope (DMIRE2; Leica, Bannockburn, IL) equipped with a cooled charge-coupled device camera (CTR MIC; Leica). Pictures were taken using Leica Qfluoro software.

Pathological Studies—Pathological studies were carried out on 10% formalin-fixed, paraffin-embedded spinal cords and brain stems filed in the Department of Neurology, Nagoya University Graduate School of Medicine. The specimens were obtained at autopsy from three sporadic cases of ALS and four sporadic PD patients. The spinal cord and brain stem specimens of these ALS and PD cases were immunohistochemically stained with antibodies against Dorfin (Dorfin-41) and VCP. Dou-

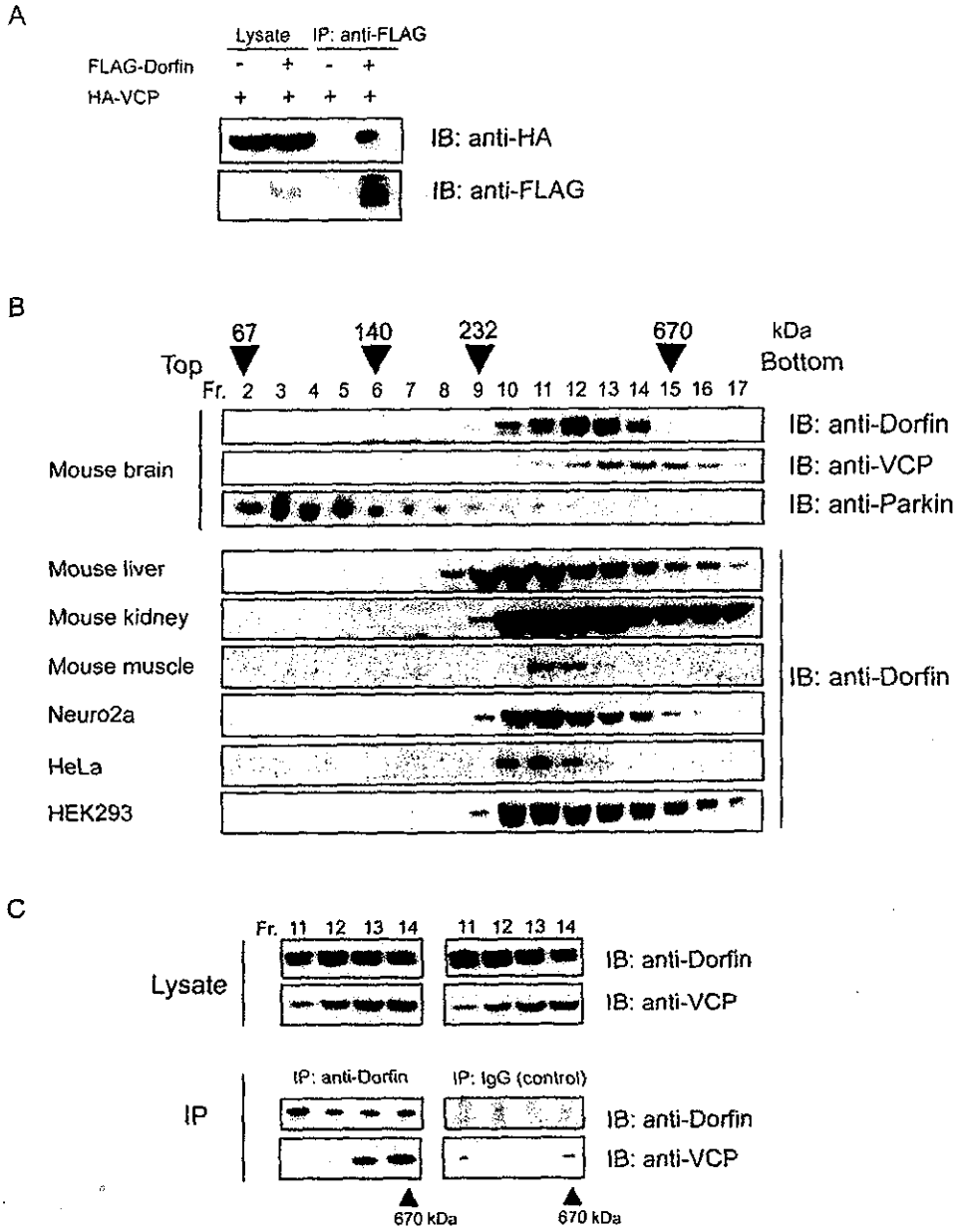

FIG. 1. ***In vivo* interaction between Dorfin and VCP.** *A*, FLAG-Dorfin and HA-VCP are co-expressed in HEK293 cells. FLAG-mock vector was used as a negative control. The amounts of HA-VCP in 10% of the lysate used are shown (*Lysate*); the rest was subjected to immunoprecipitation (*IP*) with anti-FLAG (M2) antibody. Following immunoblotting (*IB*) with anti-HA (12CA5) antibody revealed that HA-VCP was co-immunoprecipitated with FLAG-Dorfin. *B*, 5 mg of protein of various mouse tissues (brain, liver, kidney, and muscle) and 1 mg of protein of cultured cells (HEK293, HeLa, and Neuro2a) were each homogenized in 1 ml of PBS. Supernatants were fractionated by 10–40% glycerol gradient centrifugation followed by separation into 30 fractions using a fraction collector. Immunoblotting using anti-Dorfin, anti-VCP, and anti-Parkin antibodies was performed on the fractions (*Fr.*), including fractions 2–17. Endogenous Dorfin was co-sedimented with VCP in the fractions with a molecular mass of around 400–600 kDa. The positions of co-migrated molecular mass markers are indicated *above* the *panels*. *C*, immunoprecipitation with polyclonal anti-Dorfin antibody (anti-Dorfin-30) was performed on fractions 11–14 collected by glycerol gradient centrifugation analysis, where endogenous Dorfin was seen in *B*. As a negative control, immunoprecipitation with nonimmune rabbit IgG was used on the same fractions.

ble staining of identical sections was performed as described previously (7). In immunofluorescence microscopy, Alexa-488- and Alexa-546-conjugated secondary antibodies (Molecular Probes) were used. All human and animal studies described in this report were approved by the appropriate Ethics Review Committees of the Nagoya University Graduate School of Medicine.

RESULTS

Identification of Dorfin-associated Protein in the Cells—In an effort to identify protein(s) that physically interacts with Dorfin in the cells, FLAG-Dorfin was expressed in HEK293 cells and then immunoprecipitated by anti-FLAG antibody. The immunoprecipitates were eluted with a FLAG peptide and then digested with Lys-C endopeptidase (*Achromobacter* protease I), and the cleaved fragments were directly analyzed using a highly sensitive "direct nanoflow LC-MS/MS" system as described under "Materials and Methods." Following data base search, a total of 13 peptides were assigned to MS/MS spectra obtained from the LC-MS/MS analyses for the FLAG-Dorfin-

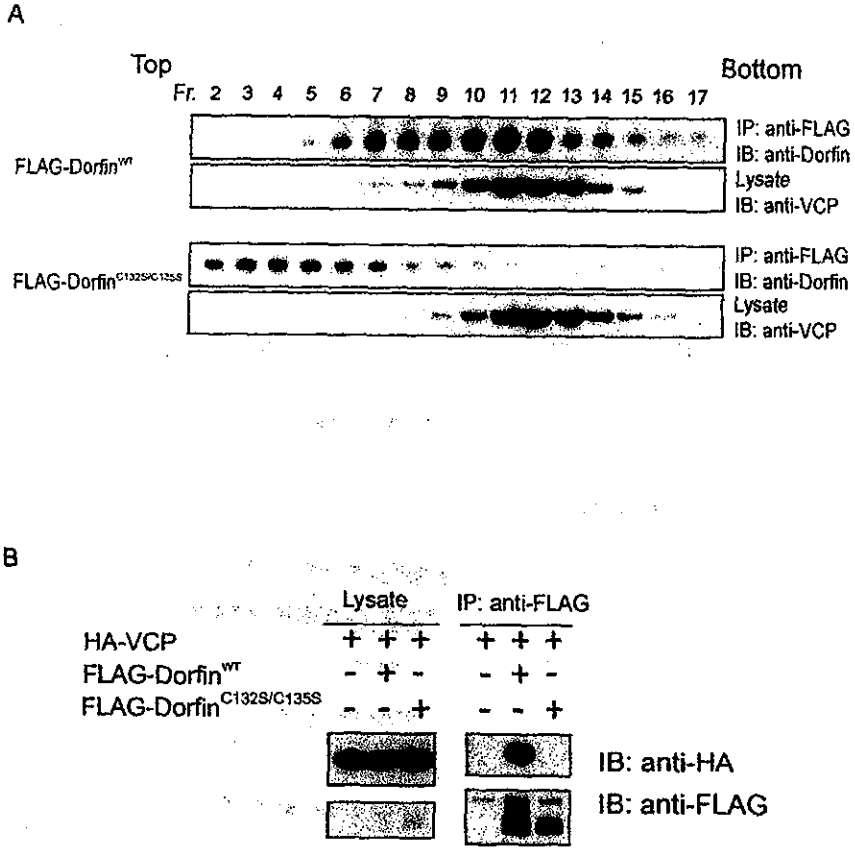

FIG. 2. **Loss of physical interaction between Dorfin$^{C132S/C135S}$ and VCP.** *A*, transfected Dorfin^{WT}, but not Dorfin$^{C132S/C135S}$ (*Dorfin$^{C132S-C135S}$*), forms a high M_r complex. Lysate of HEK293 cells overexpressed with FLAG-Dorfin^{WT} or FLAG-Dorfin$^{C132S/C135S}$ was fractionated by 10–40% glycerol gradient centrifugation. The selected fractions (*Fr.*), fractions 2–17, were subjected to immunoprecipitation (*IP*) using anti-FLAG (M2) antibody. Immunoblotting (*IB*) with anti-Dorfin antibody revealed that exogenous FLAG-Dorfin^{WT} formed a high molecular weight complex, whose peak was at fraction 11, whereas FLAG-Dorfin$^{C132S/C135S}$ migrated in fractions of smaller M_r (around fraction 7). Ten percent of the fractionated samples were shown as "lysate." *B*, Dorfin^{WT} can interact with VCP, but Dorfin$^{C132S/C135S}$ cannot. FLAG-Dorfin^{WT} or FLAG-Dorfin$^{C132S/C135S}$ and HA-VCP were co-expressed in HEK293 cells. FLAG-mock vector was used as a negative control. The amounts of HA-VCP in 10% of the lysate used are shown (*Lysate*); the rest was subjected to immunoprecipitation with anti-FLAG (M2) antibody. Following immunoblotting with anti-HA (12CA5) antibody revealed that HA-VCP was co-immunoprecipitated with FLAG-Dorfin^{WT} but not with FLAG-Dorfin$^{C132S/C135S}$.

associated complexes. These peptide data identified nine proteins as candidates for Dorfin-associated proteins. One of these identified proteins was VCP that has been proposed to have multiple functions, such as membrane fusion or endoplasmic reticulum-associated degradation (ERAD) (18–22). In the next step, we examined the relationship between Dorfin and VCP, because the latter has been reported to be linked to various aspects of neurodegeneration (15).

Dorfin Interacts with VCP in Vivo—To verify the interaction between Dorfin and VCP, FLAG-Dorfin and HA-VCP were transiently overexpressed in HEK 293 cells. Immunological analyses revealed that HA-VCP was co-immunoprecipitated with FLAG-Dorfin but not with FLAG-mock (Fig. 1*A*), confirming their physical interactions in the cells. To determine whether endogenous Dorfin forms a complex, the lysate from mouse brain homogenate was fractioned by glycerol density gradient centrifugation. Each fraction was immunoblotted with anti-Dorfin antibody. The majority of endogenous Dorfin was co-sedimented with VCP around a size of 400–600 kDa, although endogenous Parkin, which is another RING-IBR type E3 ligase (12), existed in the fractions of much lighter molecular weight (M_r) (Fig. 1*B*, *top panels*). Moreover, Dorfin was sedimented in the fractions of 400–600 kDa in other tissues, such as the liver, kidney, and muscle of mouse, and various cultured cells including Neuro2a, HeLa, and HEK293 cells (Fig. 1*B*, *bottom panels*). To determine whether endogenous Dorfin interacts with VCP, immunoprecipitation using polyclonal anti-Dorfin antibody (Dorfin-30) was performed on the fractions shown in Fig. 1*B*, *top panels*. Endogenous VCP was co-immunoprecipitated with endogenous Dorfin in the fractions of high M_r (fractions (*Fr.*) 13 and 14). No apparent band was observed when precipitated with rabbit IgG (Fig. 1*C*).

Mutations of RING Finger Domain of Dorfin Results in Loss of Dorfin-VCP Interactions—Next, we examined whether transfected Dorfin (FLAG-Dorfin^{WT}) and its RING mutant (FLAG-Dorfin$^{C132S/C135S}$), in which the two Cys residues at positions 132 and 135 within the RING finger domain were substituted for Ser residues, form a complex. The results showed overexpression of FLAG-Dorfin^{WT} in high molecular fractions (*Fr.* in Fig. 2), whose peak was between fractions 10 and 12, whereas overexpressed FLAG-Dorfin$^{C132S/C135S}$ did not consist of high molecular weight complex. Overexpression of FLAG-Dorfin^{WT} or FLAG-Dorfin$^{C132S/C135S}$ did not change the sedimentation pattern of VCP (Fig. 2*A*). Furthermore, immunoprecipitation analysis showed that FLAG-Dorfin^{WT}, but not FLAG-Dorfin$^{C132S/C135S}$, could interact with HA-VCP in HEK293 cells (Fig. 2*B*).

Dorfin Interacts with VCP in Vitro—To confirm the direct